Modeling of Energy, Water, and CO_2 Flux in a Temperate Grassland Ecosystem with SiB2: May–October 1987

G. D. COLELLO AND C. GRIVET*

Department of Plant Biology, Carnegie Institution of Washington, Stanford, California

P. J. SELLERS

Biospheric Sciences Branch, Laboratory for Atmospheres, NASA/GSFC, Greenbelt, Maryland

J. A. BERRY

Department of Plant Biology, Carnegie Institution of Washington, Stanford, California

(Manuscript received 11 June 1996, in final form 17 September 1996)

ABSTRACT

The Simple Biosphere Model, version 2 (SiB2), was designed for use within atmospheric general circulation models as a soil–vegetation–atmosphere transfer scheme that includes CO_2 flux prediction. A stand-alone version of SiB2 was used to simulate a grassland at Station 16 of the First ISLSCP Field Experiment (FIFE) located near Manhattan, Kansas, for a period of 142 days of the 1987 growing season. Modeled values of soil temperature and moisture were initialized, using field measurements from the soil profile, and thereafter updated solely by model calculations. The model was driven by half-hourly atmospheric observations and regular observations of canopy biophysics. This arrangement was intended to mimic model forcing in a GCM. Three model versions are compared: (i) a Control run using parameter values taken from look-up tables used for running the Colorado State University GCM; (ii) a Tuned run with many adjustments to optimize SiB2 to this ecosystem; and (iii) a Calibrated run, which calibrated the Control version soil to the local site and incorporated two important changes from the Tuned version. Modeled fluxes of latent heat, sensible heat, soil heat, net radiation, and net site CO_2 were compared to over 800 half-hourly observations; modeled surface and deep soil temperatures compared to 6500 observations; and three layers of modeled soil water content compared to 15 measurements of the soil water profile. Statistical methods were used to analyze these results. In the absence of water stress all three versions accurately simulated photosynthesis and canopy conductance. However, during episodes of drought, only the Tuned and Calibrated versions accurately simulated physiological control of canopy fluxes. The largest errors were encountered in the simulation of soil respiration. These were traced to problems predicting water content and temperature in the soil profile. These results highlight the need for improved simulation of soil biophysics to obtain accurate estimates of net CO_2 balance. The accuracy of the Tuned version was improved by changes that (i) allowed water extraction by roots from all soil layers, (ii) matched the soil texture specification to the site, and (iii) calibrated the expressions used for diffusion of water and heat within the soil profile.

1. Introduction

Results from a GCM are strongly influenced by the exchange of radiation, momentum, sensible heat, and latent heat between the atmosphere and the land surface. The Simple Biosphere Model (SiB) (Sellers et al. 1986) is one of the many land surface parameterizations implemented for a GCM (Garratt 1993). It is a soil–vegetation–atmosphere transfer scheme (SVATS) that uses site-specific biophysical and physiological vegetation characteristics coupled to the meteorology of the adjacent atmosphere to calculate albedo, drag, conductance, and energy partitioning of a vegetated land surface. Recently, Sellers et al. (1992a, hereafter S92a) updated SiB to include a new single-layer canopy integration scheme incorporating a leaf model based on a mechanistic description of photosynthetic CO_2 uptake and a semiempirical parameterization of stomatal conductance (Collatz et al. 1991, 1992; hereafter C91 and C92). Notably, CO_2 exchanges associated with C_3 and C_4 photosynthesis and respiration by the canopy and soil are included in this SVATS. The new version, SiB2, is more robust, has fewer adjustable parameters, and provides an improved theoretical basis for relating bio-

* Deceased 17 July 1996.

Corresponding author address: Dr. Joseph A. Berry, Department of Plant Biology, Carnegie Institution of Washington, Stanford, CA 94305.
E-mail: gcolello@mendelbio.com

physical properties of the canopy to spectral vegetation indices. The use of SiB2 within the Colorado State University (CSU) GCM is described in the series of papers by Sellers et al. (1996a, hereafter S96), Sellers et al. (1996b), and Randall et al. (1996). These simulation studies have led to new insights into the coupling of the biosphere and the atmosphere. For example, Sellers et al. (1996c) examined the significance of physiological mechanisms in the response of continental climates to increased CO_2 concentration, and Denning et al. (1995; 1996a,b) examined the role of covariation of atmospheric convection with diurnal and seasonal cycles of CO_2 exchange in determining the distribution of CO_2 within the atmosphere. The present study is part of an ongoing effort to evaluate the accuracy of land surface processing in the CSU GCM by independent validation of SiB2.

GCMs have been validated using historical averages of regional surface observations of air temperature, pressure, wind speed, precipitation, and soil water, and satellite observations of albedo and outgoing longwave (Gates et al. 1990); and seasonal cycles of atmospheric CO_2 concentration (Denning et al. 1996b). A SVATS may be evaluated directly by intercomparison of a suite of flux measurements (e.g., net radiation, evapotranspiration, sensible heat, soil heat) with simulations obtained when the model is driven with meteorological observations (Garratt et al. 1993). However, flux measurements and surface meteorology are inherently local in scale. The ''footprint'' of an eddy-correlation experiment is typically a few square kilometers, whereas a typical GCM grid box is thousands of square kilometers.

While there may be important differences in the behavior of the land surface on the scale of a GCM grid box from that of a single eddy-correlation site (see Avissar and Pielke 1989), the fundamental mechanisms that control ecosystem exchanges of energy, water, and CO_2 are not expected to be scale dependent. Furthermore, measurements at the scale of eddy-correlation experiments are presently the largest scale at which it has been possible to obtain measurements that close the water, carbon, and energy budgets of the land surface for time intervals of weeks to years. Area averaging of meteorological variables and flux observations from multiple sites located in intensively studied areas such as FIFE (Betts and Ball 1993, 1998) have been used to construct regional datasets for validation studies; for example, Viterbo and Beljaars (1995) evaluated two alternative versions of the European Centre for Medium-Range Weather Forecasts (ECMWF) land surface parameterization, run in stand-alone mode, using sitewide averages of energy flux and soil water content of the FIFE site for 140 days. Useful checks for scale-dependent effects in extrapolating from a single site to larger scales can be obtained by comparing such regional-scale simulations with direct flux measurements by aircraft (MacPherson et al. 1992); with integrative measures of flux such as soil moisture runoff (Famiglietti et al. 1992; Wood and Lakshmi 1993; Liang et al. 1994); or to remote sensing indicators of flux (Sellers et al. 1992b, hereafter S92b; 1995). However, in the context of testing the fundamental biophysical and physiological parameterizations of land surface schemes, it is not clear whether regional-scale datasets offer any substantial advantage over datasets acquired at a single site. These considerations lead us to suggest that measurements at the eddy-correlation scale presently provide the best opportunity for rigorous testing of surface schemes in land surface models.

Recent technological advances have made it possible to conduct eddy-correlation studies over long time spans. The primary motivation has been to assess whether particular ecosystems are acting as sources or sinks for atmospheric CO_2 (Wofsy et al. 1993); but these data also provide an opportunity to compare SVATS models in a stand-alone mode with observed seasonal behavior of ecosystem–atmosphere exchanges. That CO_2 is now commonly measured is a significant advantage because CO_2 is a sensitive diagnostic for physiological processes related to the control of canopy conductance (C91) and (as shown here) for soil temperature and moisture content. Some of the first work on seasonal changes in net ecosystem CO_2 flux was initiated with FIFE (Verma et al. 1992), and similar work is now in progress at dozens of sites around the world.

These advances provide a stimulus for conducting longer term tests of SVATS and for including CO_2 flux as a diagnostic in these tests. The PILPS (Project for Intercomparison of Land-surface Parameterizations Schemes) study (Henderson-Sellers et al. 1995) is making use of long-term datasets from the Cabauw grassland in the Netherlands and elsewhere to compare the outputs of SVATS models to observations of net radiation, sensible and latent heat flux, ground heat storage, and surface temperature using year-round simulations. However, CO_2 flux is not included in the PILPS study. A number of studies have attempted to simulate CO_2 flux, but most of these have been for a few days at most (Grant and Baldocchi 1992; Amthor et al. 1994; Baldocci 1994). The pioneering study of Saugier and Ripley (1975) is particularly noteworthy for simulations of CO_2 exchange and carbon balance in a Canadian grassland for two 140-day intervals. Other studies extending several months have been published by Grant et al. (1993), Chen and Coughenour (1994), and Gao (1994). McMurtrie et al. (1992) have conducted a five-year study of an Australian pine plantation. However, most of these CO_2 modeling studies have used models that are not appropriate for use as SVATS in climate models.

Our objective in this study was to exercise several features of SiB2 (particularly the capacity to simulate net CO_2 exchange, physiological response to water stress, and detailed soil water balance) over the growing season of 1987 at FIFE. The design of the simulation

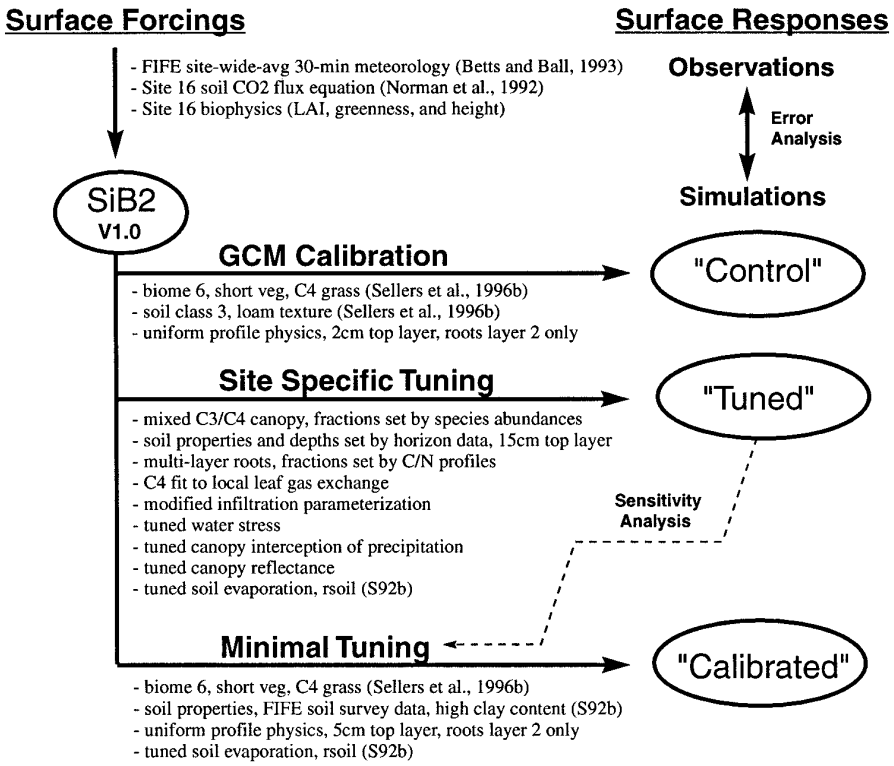

FIG. 1. The experimental design for these simulation studies. The Control configuration (run 46) used "vanilla" SiB2v1.0 with parameter values from look-up tables used to run the CSU GCM for the grid square containing FIFE. The Tuned configuration (run 45) represents our best fit of SiB2 to Site 16 allowing both code and parameter changes to SiB2v1.0. Sensitivity analysis was used to identify a few key changes resulting in the Calibrated configuration (run 89). This was similar to the Control—with minimal tuning.

experiments is outlined in Fig. 1. We made extensive use of process-level studies of photosynthesis, soil respiration, and soil evaporation to test and calibrate component models included in SiB2. For most of this work SiB2 was run in a stand-alone mode driven by meteorological observations. Its output was compared, using statistical analysis of scatter and bias, to observed fluxes of heat, net radiation, and CO_2 measured by eddy correlation at a single site (Verma et al. 1992, hereafter Site 16) conducted as part of FIFE (Sellers et al. 1988, 1992c; Sellers and Hall 1992). The FIFE experimental area is located near Manhattan, Kansas, in an area including the Konza Prairie Long-Term Ecological Research (LTER) area. The area is a tallgrass prairie ecosystem composed primarily of a mixed stand of C_3 and C_4 grasses whose abundances change during the growing season (S92b). Additional observations were made at Site 16 that were ancillary to the eddy flux experiment, including canopy biophysics, soil properties, surface temperature, soil temperature, surface reflectance, surface irradiance, and soil water. All observations used in this study, except site CO_2 flux, are available on the FIFE CD-ROM (Strebel et al. 1994). Previous papers have described the flux measurements at Site 16 (Kim and Verma 1990a, b, 1991a; Verma et al. 1992), correlated these to changes in the available soil water (Kim and Verma 1991b), examined the ability of satellite-determined vegetation indices to predict the latent heat flux from this system (Verma et al. 1993), and estimated a site carbon budget (Kim et al. 1992). These studies have highlighted strong modulation of the fluxes by physiological mechanisms presumably related to seasonal changes in the availability of soil water at this site (Stewart and Verma 1992).

We performed seasonlong (142 day) runs with Tuned, Control, and Calibrated versions of the model (Fig. 1) driven by continuous micrometeorological observations. The Tuned version produced a good match to the fluxes and soil measurements taken over the growing season. The Control and Calibrated runs illustrate that substantial differences in water and carbon balance of the ecosystem can accrue over multimonth runs with relative small differences in parameter values or model structure. The process of developing the Tuned version of the model is used to highlight areas where SiB2 needs improvement.

2. Materials and methods

a. Notation and terminology

All notations used in this paper are defined in Table A1. They follow as closely as possible those of S96. We use the term *prognostic* to refer to the SiB2 variables whose values are retained from one time step to the next (T_c, T_g, T_d, W_1, W_2, W_3, M_c, M_g, and g_c).

b. Site description

What we refer to in this study as ''Site 16'' is equivalent to FIFE grid 4439 (collocated 1987 station IDs 16, 11, 18, 73, and 106). The site has an elevation of 443 m and was centered at 39°03′06″ lat, −96°32′28″ long. It was described as ungrazed, burned on 15 April, mostly level, but with at least 7% north-facing steep slopes. Its species composition was listed in detail by Kim and Verma (1991a). They described it as being dominated by the C_4 grasses *Andropogon geradii, Sorghastrum nutans,* and *Panicum virgatum*. The soil column is about 140 cm in depth changing from silty–clay–loam to clay to gravel to impermeable bedrock.

c. Short-term calibration runs

Thirteen short-term simulations of Site 16 were conducted ranging in duration from 4 to 58 simulated hours. These periods corresponded to times when the eddy flux station was operational at Site 16. Here g_c was initialized to a steady-state value consistent with the conditions of the first time step [see S96, Eq. (C.16)]; M_c and M_g were intialized to zero; W_1, W_2, W_3 were set to the same water content using an average of the start-day's 0–140 cm water content from Verma et al. (1993); and T_c, T_g, and T_d were initialized using field observations. These short-term simulations were conducted as part of the development of the Tuned version described below.

d. Growing season continuous runs

Three seasonlong SiB2 simulations of Site 16 were conducted for the 142-day interval, 28 May through 16 October 1987. They are identified by the version names Control, Calibrated, and Tuned (Fig. 1) and correspond to lab run numbers 18.46, 18.89, and 18.45, respectively. The Tuned version included several code modifications to SiB2v1.0 (see the Appendix). There were also version differences in parameter values, which are listed as separate columns in the parameter tables presented below. All versions were driven by the same meteorological observations consisting of $S\downarrow$, $L\downarrow$, e_m, T_m, P, and u_m (section 2f). Linear interpolation of the 30-min driver data into 6-min intervals was performed at run time. This allowed a more stable solution of the SiB2 energy and soil water budgets. The variable g_c was initialized to a steady-state value consistent with the conditions of the first time step; M_c and M_g were intialized to zero; and W_1, W_2, W_3, T_c, T_g, and T_d were initialized using field observations.

e. Statistical comparisons of simulations with observations

We used a set of statistical techniques similar to Baldocchi (1992), which included a consideration of flux uncertainties. Fifteen simulation output variables were compared to corresponding observations (λE_m, H_m, G, R_n, A_m, W_1, W_2, W_3, $S\uparrow$, $L\uparrow$, T_{skin}, $T_{0\text{–}5\text{cm}}$, $T_{10\text{cm}}$, $T_{50\text{cm}}$, and f_w). The following comparison statistics were calculated where observations are o_i, simulations are s_i, and the total number of observations are n

1) Standard error of the estimate (SEE, units are the same as o_i):

$$\text{SEE} = \sqrt{\frac{\sum_{i=1}^{n} (s_i - o_i)^2}{n - 2}}. \tag{1}$$

2) ''Normalized'' SEE, an estimate of relative uncertainty (unitless, equivalent to the rms deviation divided by the rms observation):

$$\text{NSEE} = \sqrt{\frac{\sum_{i=1}^{n} (s_i - o_i)^2}{\sum_{i=1}^{n} (o_i)^2}}. \tag{2}$$

3) ''1:1'' Linear regression: The slope (BIAS), intercept (INTER), and their standard errors (SE) were calculated for the unconstrained linear regression line of all (o_i, s_i) data pairs. Ideally the BIAS should be 1.0, and the INTER should be 0.0. The BIAS and INTER were tested for significant differences from these ideal values using a t test.

f. Meteorological dataset

To produce continuous meteorological driver-data for Site 16 simulations, we started with a FIFE areawide dataset (Betts and Ball 1993). The dataset was generated by averaging observations from all available FIFE automated meteorological stations (AMS), which measured conditions at 30-min intervals for days 145–288 of the 1987 growing season. Some short gaps had to be filled by linear interpolation and with data from the nearby LTER site and FIFE flux stations. Time was corrected from UTC to solar time by subtracting 6 h 26 min. We were concerned that the areawide-average data might be inconsistent with the micrometeorology of Site 16 since there was significant variability in the micrometeorology across the entire FIFE site. Therefore, discontinuous micrometeorological observations taken at Site 16 (section 2g) and at a site with similar aspect (E. Smith, Station 2, FIFE-CD-ROM) were used to check

for inconsistencies between the areawide averages and the individual sites. In general the data were consistent, but we found that it was possible to improve the agreement by applying the correction factors 0.95, 0.93, and 0.75 to the areawide $S\downarrow$, $L\downarrow$, and u_m, respectively. The comparison of u_m should have taken into account the differing heights of the AMS (5.4 m) and eddy flux (2.5 m) stations, which we only became aware of after the simulations had been performed; however, the 0.75 correction factor used was probably adequate. Vapor pressure (e_m) was calculated from areawide T_m and T_{wet}. Also extracted from the areawide dataset was T_{skin}, $T_{10\text{cm}}$, $T_{50\text{cm}}$, and $S\uparrow$ for comparison with SiB2 simulation output. We found that $L\uparrow$ (used for comparison with SiB2 simulation output) could be much more accurately estimated as a function of areawide T_{skin} using the standard blackbody radiation equation, than as a residual of areawide R_n, $S\downarrow$, $L\downarrow$, and $S\uparrow$.

g. Eddy flux dataset

This dataset was constructed from eddy flux station data collected by S. Verma during 1987 at station 16 and were used for comparison with SiB2 simulation output. Here λE_m, H_m, G, R_n, and $T_{0-5\text{cm}}$ were obtained from the FIFE CD-ROM, and A_m was obtained from S. Verma. The method of data collection was described in Kim and Verma (1991b). The dataset covers the breadth of the growing season, but it contains several large gaps. Thirteen representative periods were selected from the dataset for comparison with the short-term SiB2 runs. For the seasonlong SiB2 runs all available eddy flux data were used for comparison with SiB2 output. Time was corrected from local daylight savings time to solar time by subtracting 1 h 26 min. For the Tuned version of SiB2 we calibrated $S\downarrow_{\text{PAR}}$ calculations against the meteorological observations taken at Site 16, by adjusting $S\downarrow_{\text{PARfac}}$ (Table 1).

h. Soil water dataset

These data are all shown in Fig. 2. Neutron probe measurements of soil water content centered at 20 cm (10–25 cm), 30 cm (25–35 cm), 40 cm (35–45 cm), 50 cm (45–55 cm), 60 cm (55–70 cm), 80 cm (70–90 cm), 100 cm (90–110 cm), 120 cm (110–130 cm), and 140 cm (130–140 cm) were conducted several times during the season by the FIFE staff. They supplemented these data near the surface by gravimetric measurements of soil water centered at 2.5 cm (0–5 cm) and 7.5 cm (5–10 cm), which were converted to volumetric soil water content using soil density measurements. The vertical bars mark the estimated range of soil water content available to the canopy (field capacity to wilting point). At different times during the growing season, the soil water profile shows very dynamic changes near the soil surface in response to the timing and quantity of precipitation received at the site. On the other hand, water in the subsoil (>1 m) was constant and apparently not drawn down by the plants even during periods of severe drought. To check on the consistency of the site hydrology measurements, we compared changes in the total moisture stored in the soil (ΔW_{soil}) to the measured soil inputs (precipitation, 249.9 mm) and outputs (latent heat by eddy flux) integrated over the interval from yearday (DOY) 183 to 289 (322.3 mm). This analysis was not exact since we had to interpolate through intervals with no evaporation measurements, and we as-

TABLE 1. Miscellaneous site parameter values. The symbols and units are defined in Table A1.

Parameter	Tuned	Control[a]	Calibrated[a]
Latitude	39.0	*	*
Longitude	−95.0	*	*
c_m	34.0	*	*
$S\downarrow_{\text{PARfac}}$	0.9	—	—
$M_{c_{\max}}$	0.01×10^{-4}	1.0×10^{-4}	1.0×10^{-4}
$M_{g_{\max}}$	2.0×10^{-3}	2.0×10^{-3}	2.0×10^{-3}
a_{Rg}	1.044	*	*
a_{rsoil}	8.9	—	8.206
b_{rsoil}	4.255	—	4.255
C_{soilfac}	0.5	—	—
$\alpha_{\text{V,l}}$	0.2	0.105	0.105
$\alpha_{\text{V,d}}$	0.3	0.36	0.36
$\alpha_{\text{N,l}}$	0.55	0.58	0.58
$\alpha_{\text{N,d}}$	0.5	0.58	0.58
$\delta_{\text{V,l}}$	0.04	0.07	0.07
$\delta_{\text{V,d}}$	0.1	0.22	0.22
$\delta_{\text{N,l}}$	0.2	0.25	0.25
$\delta_{\text{N,d}}$	0.3	0.38	0.38
a_{sV}	0.1	0.11	0.11
a_{sN}	0.2	0.225	0.225
D_1	0.15	0.02	0.05
D_2	0.75	0.98	0.90
D_3	0.50	0.50	0.45
D_r	D_T	1.00	0.95
D_T	1.40	1.50	1.40
f_{root1}	0.455	0.0	0.0
f_{root2}	0.54	1.0	1.0
f_{root3}	0.005	0.0	0.0
Ψ_c	—	−200	−140
W_{isp}	0.27	—	—
W_{cap}	0.15	—	—
V	0.95	1.0	1.0
G_1	1.449	*	*
G_4	11.785	*	*
l_1	0.2	*	*
l_w	0.01	*	*
χ_L	−0.3	*	*
z_m	2.25	*	*
$G(\overline{\mu})/\overline{\mu}$	0.73–1.00	*	*
L_T	1.34–3.51	*	*
N	0.35–0.91	*	*
z_2	0.29–0.58	*	*
z_c	$(0.4z_2 + 0.08)$	*	*
z_1	$(0.16z_2 - 0.028)$	*	*
z_s	$(0.018z_2 - 0.0044)$	*	*
f_{c3}	0.23–0.40	0.0	0.0
f_{c4}	0.60–0.77	1.0	1.0

[a] Obtained from the CSU GCM (Sellers et al. 1996b, Table 5a, biome 6) except as noted in the text.

— Not applicable.

* Set the same as Tuned.

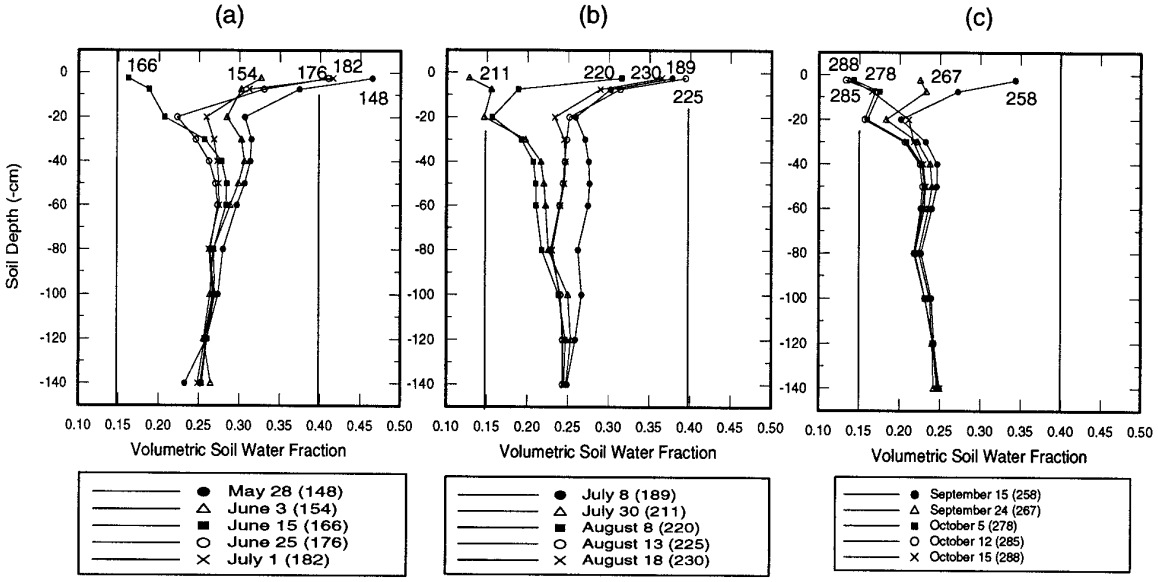

FIG. 2. Profiles of soil water content at Site 16 in 1987: (a)–(c) volumetric soil water profiles covering the dates 28 May–15 October. Separate profiles are identified by symbols as well as the yearday (DOY). Left and right vertical dark lines represent the soil water contents at the permanent wilting point and at field capacity, respectively (Verma et al. 1989).

sumed that runoff and drainage (not measured) were negligible. Nevertheless, the changes in soil water measured at nine times during the interval matched ($\overline{x}$ = 0.3 ± 9.8 mm) the integrated water budget.

i. Time-invariant miscellaneous site parameters

These can all be found in Table 1. With a few minor exceptions Control and Calibrated parameter values were all obtained from Sellers et al. (1996b). Latitude and longitude were obtained from Verma et al. (1993). Initial values of Tuned leaf reflectance and transmittance were estimated from Walter-Shea et al. (1992). These were modified by experimentation during SiB2 calibration runs to produce better matches to the following light observations: $S\uparrow$ (section 2f); $S\uparrow_{\mathrm{PAR}}$ and $S\uparrow_{\mathrm{NIR}}$ (Site 16 surface MMR data, FIFE-CD-ROM); and $S\uparrow_{\mathrm{PAR}}$ and $S\downarrow_{\mathrm{PAR}}$ (Site 16 UNL light-bar data, FIFE-CD-ROM). Tuned soil reflectance values were set as in S92b. Parameters C_{soilfac}, $M_{c_{\max}}$, and $M_{g_{\max}}$ were optimized from their Control values during Tuned experimental runs. The Tuned canopy cover fraction was obtained from Dr. P. Sellers. Tuned c_m was left at its Control value. To assign the SiB2 soil layers thicknesses (D_1, D_2, and D_3) for the Tuned version, soil horizon data were grouped by similar textures. The fraction of "functional roots" in each layer was defined as that layer's fraction of the total organic matter in the soil profile. Vegetation cover (V) for the Tuned version was set to a value slightly less than 1.0, based on the gap frequency revealed by vertical photographs of Site 16. Calibrated Ψ_c and Tuned W_{isp} and W_{csp} were set using fitting procedures.

TABLE 2. Soil hydraulic site parameter values. The symbols and units are defined in Table A1.

Parameter	Tuned	Control[a]	Calibrated[b]
K_{infil}	20.0×10^{-6}	—	—
ϕ_s	0.0	10.0	10.0
θ_s	—	0.45	0.43
θ_{s1}	0.46	—	—
θ_{s2}	0.48	—	—
θ_{s3}	0.39	—	—
K_s	—	7.0×10^{-6}	1.66×10^{-6}
K_{s1}	1.7×10^{-6}	—	—
K_{s2}	1.2×10^{-6}	—	—
K_{s3}	1.0×10^{-6}	—	—
Ψ_s	—	−0.15	−0.50
Ψ_{s1}	−0.15	—	—
Ψ_{s2}	−0.17	—	—
Ψ_{s3}	−0.16	—	—
B	—	5.39	8.00
B_1	8.0	—	—
B_2	10.0	—	—
B_3	10.0	—	—

[a] Obtained from the CSU GCM [Sellers et al. 1996b, Table 4 (class 3) and Table 5b].
[b] Obtained from S92b, Table 1c.

j. Time-varying biophysical site parameters

The biophysical parameters L_T, N, f_{c3}, and f_{c4} (S92b) and z_2 (FIFE CD-ROM) are listed in Table 1 with their range of reported values. Daily values used in the simulations (available from author J. Berry) were derived by interpolation of the reported intermittant values. S92b derived their f_{c3} and f_{c4} data from species abun-

dance data. Here L_T was calculated by dividing L_G by N, both from S92b. Their L_G data were derived from Verma et al. (1992), and their N data from dried green and total biomass data measured by the FIFE staff. Unfortunately, a comparison of L_G data from S92b with L_G data measured by the FIFE staff revealed major differences possibly due to reported leaf curling complications. This variance in Site 16 leaf area measurements has been analyzed in detail by Kim et al. (1989). To be consistent with the other biophysical data we used only L_G values from S92b. Intermittant measurements of z_2 at Site 16 were made by the FIFE staff. Here, z_m was obtained from Verma et al. (1993). The l_l, l_w, G_1, G_4, and χ_l aerodynamic constants were obtained from Dr. P. Sellers. The z_c, z_1, and z_s (not measured in the field) were given daily values as a function of z_2, using the equations in Table 1, which were obtained from P. Sellers. Note in Table 1 the special case, where Control and Calibrated f_{c3} and f_{c4} were set to constant (time invariant) values; otherwise all versions shared the same biophysical values.

k. Time-varying aerodynamic site parameters

Values of the SiB2 run-time aerodynamic parameters (z_0, d, C_1, C_2, RB1, RB2, h_a, G_2, and G_3) were calculated off-line for each day of the simulations, using the site surface characteristics L_T, l_l, l_w, χ_l, V, z_m, z_2, z_c, z_1, z_s, G_1, and G_4 (Table 1), and a special preprocessing program called MOMOPT (P. Sellers). The theory behind MOMOPT (a first-order approximation to a second-order closure scheme) is presented in Sellers et al. (1989, appendix A). Note the Tuned value of V was used in MOMOPT, so there would be no difference in aerodynamics between the versions.

l. Time-varying solar angle term (the Π factor)

To calculate integrated canopy performance SiB2 scales canopy top leaf net photosynthesis (A_c) by the factor Π, which is linearly related to canopy FPAR as described by S92a. SiB2 requires the daily estimation of Π, which in turn requires the daily estimation of the average solar angle term $G(\overline{\mu})/\overline{\mu}$. Table 1 lists the range of values of $G(\overline{\mu})/\overline{\mu}$ for all the simulation starting days shared by all the SiB2 versions. One of the advantages of Π is that it should be directly estimatable using the remotely sensed simple ratio (SR) vegetation index; however, for both our short-term and long-term simulations, Π was estimated using ground-based measurements as in S96 [Eqs. (C.19)–(C.24)]. Equation (3) summarizes the ground-based functional dependencies of Π, which include daily canopy biophysics (Table 1) and a calculation of daily average solar angle. The full equation set for Π can be found in S92a:

$$\Pi = f(L_T, N, V, \omega_v, G(\overline{\mu})/\overline{\mu}), \quad (3)$$

where $\overline{\mu}$ is the daily average of μ, the time-varying sine of the solar elevation angle.

TABLE 3. Plant physiology site parameter values. The symbols and units are defined in Table A1.

Parameter	Tuned		Control/Calibrated
	C_3[a]	C_4[b]	C_4[c]
ϵ_3	0.08	—	—
ϵ_4	—	0.05	0.05
V_{max0} canopy	120	30	30
V_{max0} leaf (*P. virgatum*)	—	26	—
V_{max0} leaf (*S. nutans*)	—	25	—
V_{max0} leaf (*A. geradii*)	—	19	—
s_1	0.3	0.27	0.3
s_2	39.8	41.0	39.8
s_3	—	0.3	0.2
s_4	—	14.8	14.8
R_d	2.4	2.0	0.45
f_d	0.02	0.066	0.015
R_{dQ10}	2.0	1.74	2.0
s_5	0.30	0.30	1.3
s_6	55	55	54.8
w_{s1}	0.2	—	—
w_{s2}	9.8	—	—
β_{ce}	0.96	0.8	0.8
β_{ps}	0.96	0.96	0.95
m	9.0	3.62	4.0
b	0.01	0.045	0.04
k_g	0.0005	0.0005	0.0005

[a] These values were taken directly from C91 (*Glycine max*). The temperature inhibition constants have been converted to equation forms like those in S96. V_{max0} was set as described in the methods.

[b] These values ended up being slightly different from the *Zea mays* values of C92 as described in section 2.

[c] These values were taken directly from C92 (*Zea mays*) with minor changes. They were the same for Control and Calibrated.

m. Time-invariant soil hydraulic site constants

Table 2 lists the values of our Site 16 SiB2 soil hydrology parameters. Control and calibrated parameter values were obtained from the indicated references. Tuned values were set using soil survey horizon data and Clapp and Hornberger (1978) hydraulic parameters (CH hereafter). Average values of percent clay, percent silt, and percent sand for the SiB2 soil layers corresponding to D_1, D_2, and D_3 were calculated from data on the soil profile weighted by thickness. SiB2 B, Ψ_s, K_s, and θ_s were set using the CH $\overline{b}$, $\overline{\psi}_s$ (log), K_s, and $\overline{\theta}_s$ columns respectively except that θ_s was corrected for the presence of rocks. Parameters K_{infil} and ϕ_s were optimized during SiB2 Tuned runs.

n. Time-invariant plant physiology site parameters

Table 3 lists the plant physiology parameters. Control and Calibrated C_4 and Tuned C_3 parameter values were obtained from the indicated references. Tuned C_4 values were set using a SiB2 leaf gas exchange chamber simulation mode to simulate leaf-level observations. The

energy and water budget calculations of the main SiB2 model were by-passed, and parameter values for temperature T_a, humidity e_a, incident par $S_{\mathrm{PAR}}\downarrow$, CO_2 concentration c_a, and boundary layer conductance g_b were prescribed using a special input file. To construct leaf response curves, one of these parameters was stepped over a range of values, while the other parameters were held constant. To collapse the canopy to a single leaf, canopy light extinction parameters were set to 1.0 (N, L_T, Π). For each new value of the stepped parameter the photosynthesis submodel was iterated until photosynthesis and stomatal conductance came to steady state.

3. Results and discussion

a. Calibration from process-level studies

SiB2 uses the C_3 and C_4 leaf models for photosynthesis and stomatal regulation (C91 and C92) and a canopy integration scheme, which relates the response of the canopy to that of single leaves at the top of the canopy (S92a), to calculate canopy net photosynthesis and canopy resistance to water vapor transport. Extensive measurements of C_4 photosynthesis at the leaf scale were conducted during the FIFE experiment (Polley et al. 1992) and as part of the LTER project (Knapp 1985). These data provided an opportunity to calibrate the physiological constants used by SiB2. The C_4 photosynthesis parameters were fit to measurements of leaf photosynthesis, which were digitized from the published curves. Figures 3a–c illustrate leaf responses of the C_4 grass *Panicum virgatum* to variations in light and intercellular CO_2 (from Polley et al. 1992) and leaf temperatures (from Knapp 1985). Simulations (solid lines), using SiB2 in its leaf chamber mode (section 2n), are shown compared to observations (symbols). Similar results were obtained with two other C_4 species (*Sorgastrum nutans* and *Andropogon gerardii*). The parameters that were fit included the dark respiration coefficients (R_d, $R_{dQ_{10}}$, s_5, s_6), the colimitation curvature coefficients (β_{ce} and β_{pe}), and the rubisco low and high temperature inhibition constants (s_1, s_2, s_3, s_4). Figure 3d shows a combined plot of all leaf-scale measurements and simulations. A linear regression line for this plot, passing through the origin, has a slope of 1.0 with an r^2 of 0.98 indicating a good fit. The Tuned physiological parameter values were not substantially different from those of Control (Table 3) except for the dark respiration rates. The stomatal conductance equation parameter values were taken directly from Polley et al. (1992). The primary data were not presented in their article, so we accepted their stated regression values of $m = 3.6$ and $b = 0.045$, which are similar to 4.0 and 0.04 respectively as used in the Control version.

Soil respiration was estimated using the process model of Norman et al. (1992). Equation (A7) predicts CO_2 flux at the soil surface as a function of canopy development, soil moisture, and soil temperature.

b. Calibration of canopy capacity from site-level measurements

Figure 4 shows the results of simulations of site-scale energy and CO_2 fluxes for three consecutive days (dashed lines) compared with observations (points). Note that net site CO_2 flux simulations and observations include soil respiration. These simulations cover a period (4–7 June, yeardays 155–158) early in the growing season following heavy rains and mild evaporative conditions. The availability of soil water was near its highest point of the season but still lower than field capacity (Fig. 2). Temperatures were mild, the humidity was moderate, and we assume there was no water stress.

The value of the major adjustable parameter of the physiological model, C_4–V_{max0}, was adjusted to fit the observations. A value of 30 μmol m^{-2} s^{-1} for a leaf at the top of the canopy resulted in good agreement of the canopy model with the observations. The simulations shown in Fig. 4 are for a mixed canopy. Lacking any measurements of photosynthesis of C_3 species at FIFE, the C_3–V_{max0} of rubisco was set to a plausible value of 120 μmol m^{-2} s^{-1} (C91). Similar values of C_4–V_{max0} were obtained whether the canopy was modeled as a pure stand of C_4 species or the real mixture (39% C_3 and 61% C_4 species). This compares with a weighted-average leaf-level calibration value of 23 μmol m^{-2} s^{-1} [weighted by the Kim and Verma (1991b) reported abundance percentages], to the 35 μmol m^{-2} s^{-1} reported for corn (C92), and is identical to the value selected for GCM simulations of C_4–grassland ecosystems.

One caveat with respect to the V_{max0} calibrations is that any error in the SiB2 canopy integration factor Π [see S96, Eqs. (C.19), (C.21), (C.22)] will appear in the apparent V_{max0} in the canopy-scale calibrations. We prescribed Π from field measurements of canopy biophysics [Eq. (3)]. These Π values appeared reasonably consistent with a few test values obtained from local satellite observations (data not shown). However, given the overall uncertainty, a discrepancy of 30% between V_{max0} values obtained by calibration at the leaf and canopy scales provide support for the hypothesis presented by S92a that process-level studies of leaf physiology can be used to calibrate models intended for simulation of canopy processes. It is also encouraging and noteworthy that the model, using the calibrated value of C_4–V_{max0}, correctly simulated water and energy fluxes at the site without further tuning (Fig. 4).

c. Calibration of the soil water stress parameter from site-level measurements

SiB2 contains a variable for soil water stress, f_w, which attenuates the value of V_{max0} (of both C_3 and C_4 species) as soil water availability falls [see S96, Eq. (C.17)]. This is intended to reproduce the effect but does not represent the mechanism of water stress. Earlier

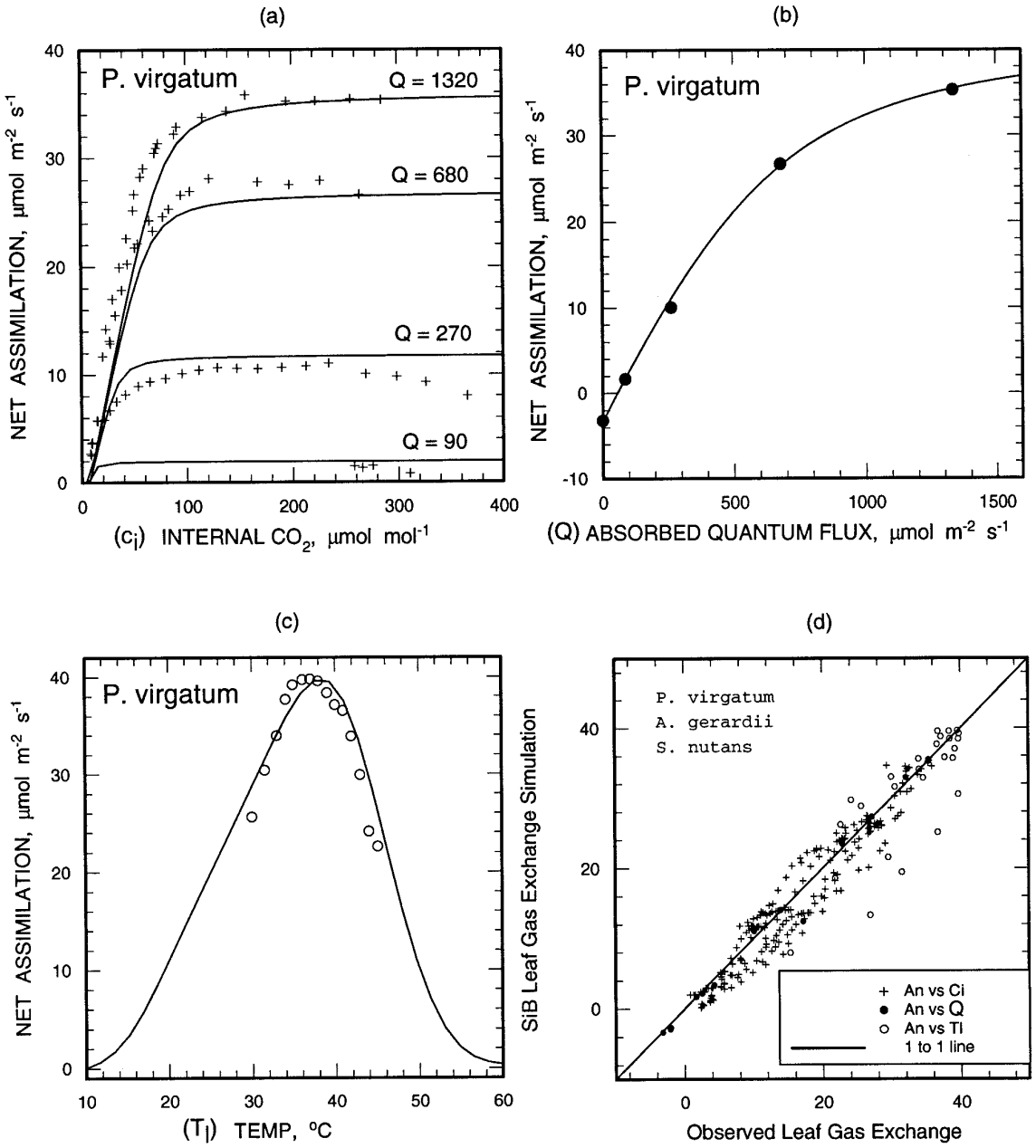

FIG. 3. Leaf-level studies of gas exchange responses (data points) and simulations using the Tuned version's leaf chamber simulation mode (solid lines). *P. virgatum* is used as an example in panels (a)–(c): (a) net photosynthesis as a function of intercellular CO_2 at four different absorbed light levels (Q) in μmol m^{-2} s^{-1} [data from Polley et al.(1992), Fig. 1]; (b) net photosynthesis as a function of absorbed quantum flux at saturating intercellular CO_2 [data from Polley et al. (1992), Fig. 2]; (c) net photosynthesis as a function of leaf temperature at rate-saturating values of Q [data from Knapp (1985), Fig. 2]. Corresponding plots were done for *A. gerardii* and *S. nutans* also (not shown), and the data were pooled into panel (d) a one-to-one plot of modeled versus observed net photosynthesis. The pluses are from plots of net photosynthesis as a function of intercellular CO_2. The solid circles are from plots of net photosynthesis as a function of Q. The open circles are from plots of net photosynthesis as a function of temperature. Different values of V_{max0} were used for each species (Table 3). The slope of a linear regression line fitted to the data points and passing through the origin is 0.96 with an r^2 of 0.98.

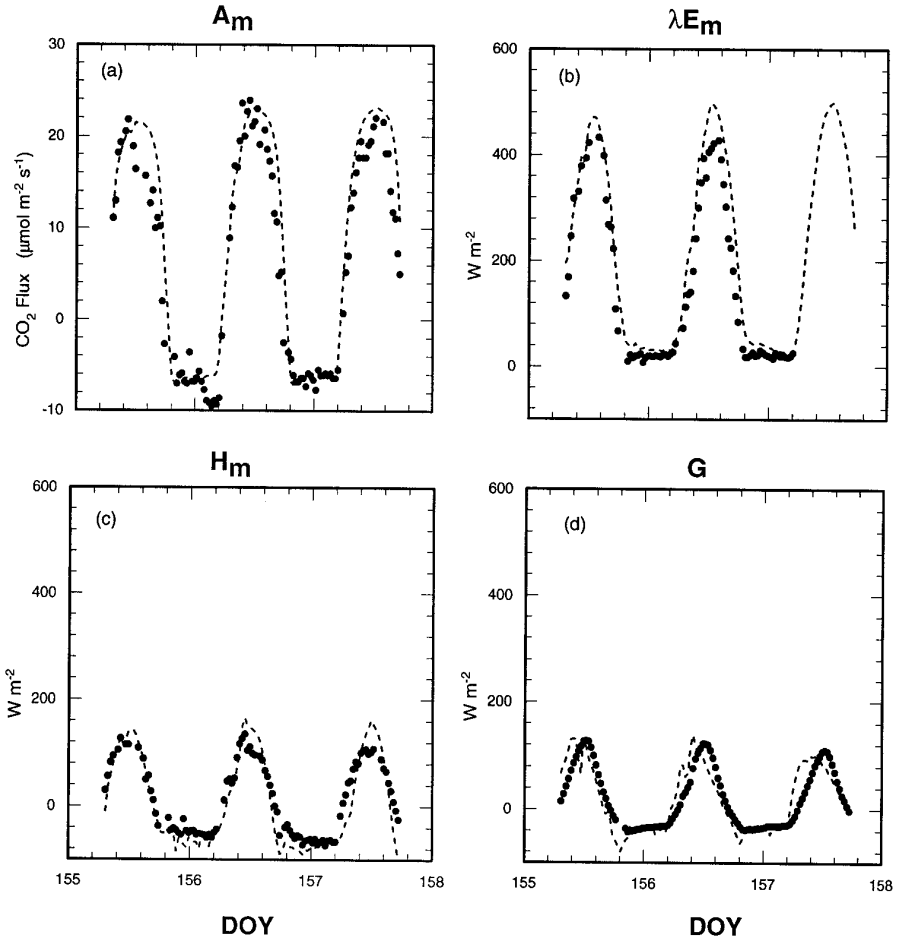

FIG. 4. Short-term simulations (dashed lines) and eddy correlation observations (solid circles) of site fluxes from the period 4–7 Jun 1987 (DOY 155–158). The simulations were performed using a preliminary form of the Tuned version. The canopy C_4–V_{max0} was set to 30 μmol m^{-2} s^{-1}.

studies have highlighted strong modulation of the fluxes by physiological mechanisms presumably related to seasonal changes in the availability of soil water at this site (Stewart and Verma 1992; Verma et al. 1993). No direct physiological studies of water stress responses were reported from FIFE. We made use of measurements of soil moisture at the site and seasonal changes in net site CO_2 flux to calibrate the water-stress responses of SiB2.

Figure 5 presents diurnal plots of observed and simulated net site CO_2 flux (A_m) for six representative periods from a total of 13 periods used for calibrating the response to water stress. Figure 6 presents plots of observed and simulated energy fluxes (R_n, λE_m, H_m, and G) corresponding in time to Fig. 5. At the beginning of the season (panel a), climate, canopy, and soil water conditions were optimal; A_m was at peak levels, and surface energy exchange was dominated by λE_m (H_m was very low). By 10 October (panel f) virtually all photosynthetic activity was gone. The soil was dry, temperatures were low, the canopy was in senescence, and H_m dominated surface energy exchange. We assume here that water stress accounts for all variation in canopy and soil CO_2 flux over the season that could not otherwise be accounted for by SiB2 using the above calibration under unstressed conditions. For each short-term run, the model was initialized and driven from observed soil moisture, canopy biophysics and meteorology. The water stress parameter (f_w) was adjusted for each of the 13 short-term simulation periods (while keeping V_{max0} constant) to fit the net CO_2 flux. The resulting values of f_w for all 13 short-term periods are plotted in Fig. 7 as a function of the yearday (DOY). Note that in SiB2 f_w is normally calculated as a function of prognostic soil moisture. The "fitted" values of f_w give a set of empirical "observations" that were used to calibrate SiB2's functional water stress response. Note that only f_w was tuned.

The fitted simulations (shown as lines on Figs. 5 and

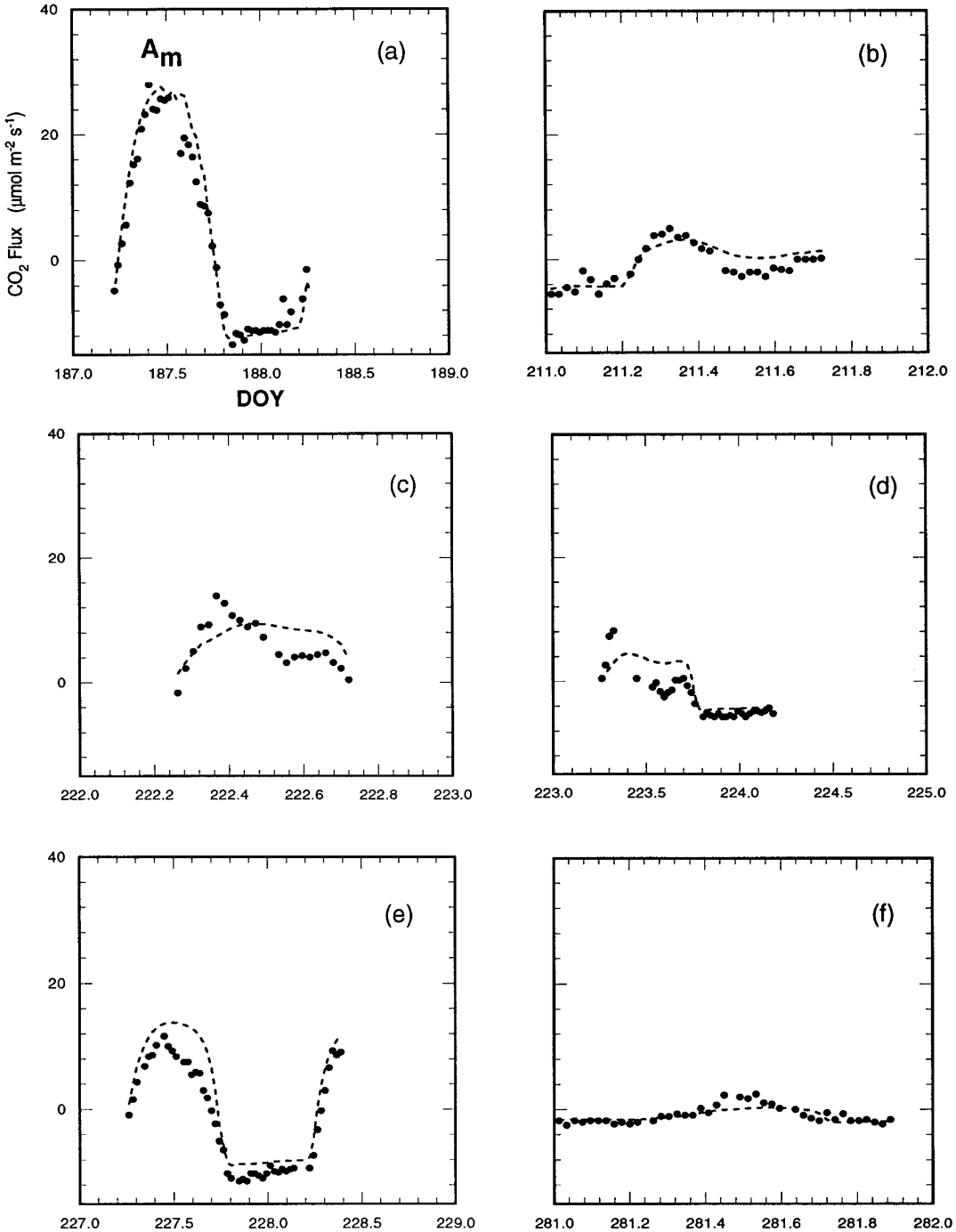

FIG. 5. Short-term simulations (dashed lines) and eddy-correlation observations (solid circles) of net site CO_2 flux (A_m). The simulations were performed using the same value of the C_4–V_{max0} as in Fig. 4. The soil water stress factor (f_w) was adjusted to fit simulations to observations. Six examples are shown from a total of 13 intervals: (a) 6–8 Jul (DOY 187–189), nearly full green canopy (L_G = 2.2) and no soil moisture stress (f_w = 1.0); (b) 30 Jul (DOY 211), still nearly full green canopy (L_G = 2.1) but with very high soil moisture stress following the first dry down period (f_w = 0.20); (c) 10 Aug (DOY 222), a slightly senescent green canopy (L_G = 1.8) but with some recovery from the first dry down period following a series of rain events (f_w = 0.50); (d) 11–12 Aug (DOY 223–224), still a slightly senescent green canopy (L_G = 1.8) but with very high soil moisture stress following the second dry down period (f_w = 0.27); (e) 15–16 Aug (DOY 227–228), still a slightly senescent green canopy (L_G = 1.7) but with nearly complete recovery from the second dry down period following a major series of rain events (f_w = 0.72); (f) 8 Oct (DOY 281), nearly complete canopy senescence (L_G = 0.7) coupled with very high soil moisture stress following the third dry down period (f_w = 0.30).

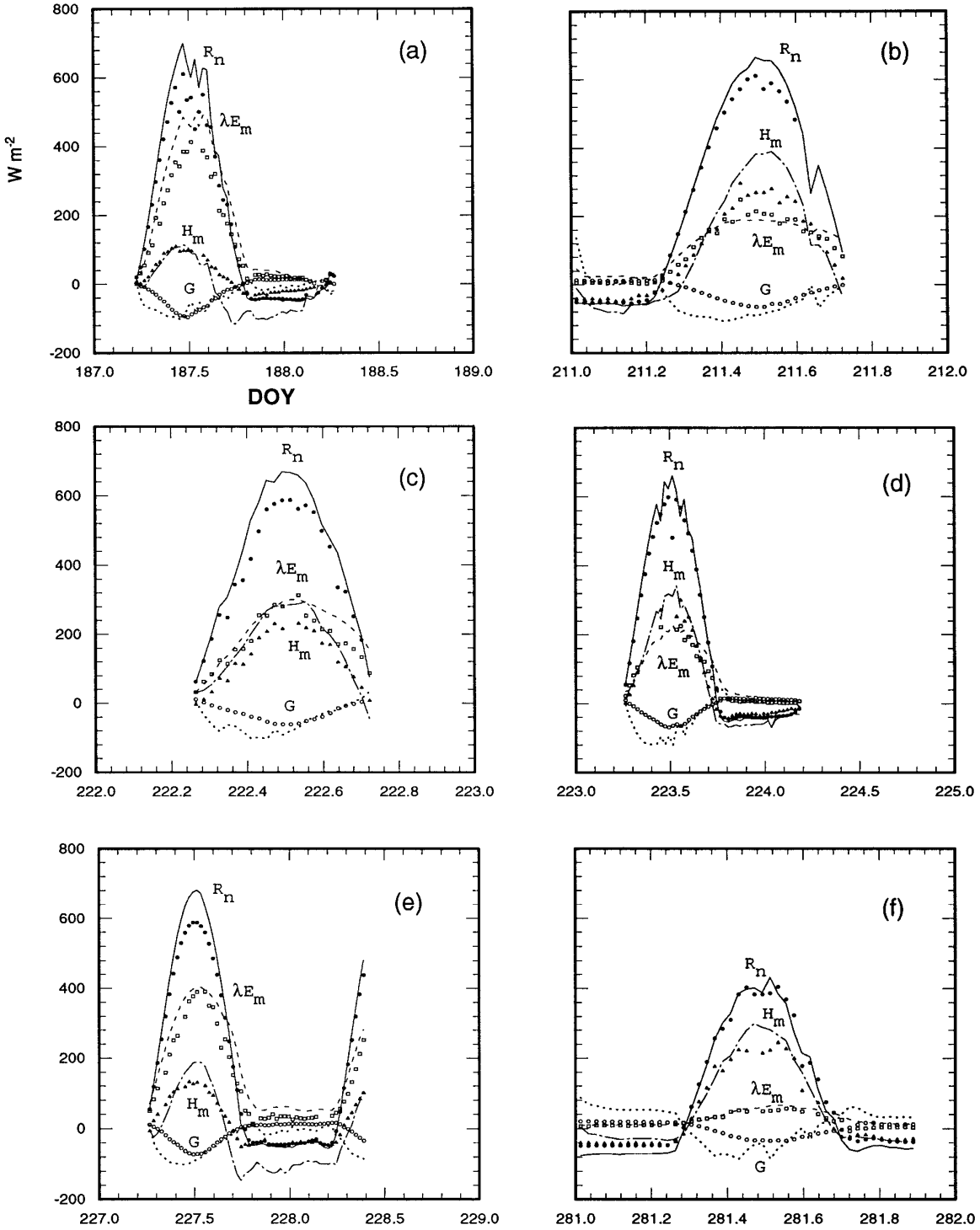

FIG. 6. Energy budget simulations and observations associated with the short-term model runs shown in Fig. 5: R_n simulations (solid lines); R_n observations (solid circles); λE_m simulations (dashed lines); λE_m observations (open squares); H_m simulations (dash–dot lines); H_m observations (solid triangles); G simulations (dotted lines); and G observations (open circles).

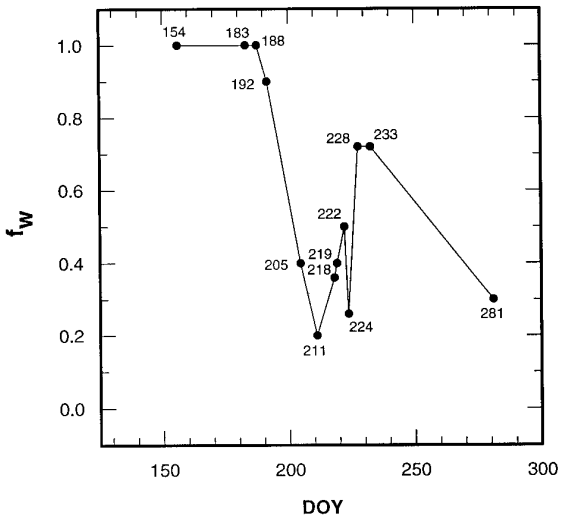

FIG. 7. "Observations" of the soil water stress factor (f_w) obtained by the best fit of 13 short-term simulations to observed fluxes (cf. Figs. 5 and 6) plotted against the DOY. Note that the lines connecting measurements may not represent the true time course of changes in water stress during these intervals.

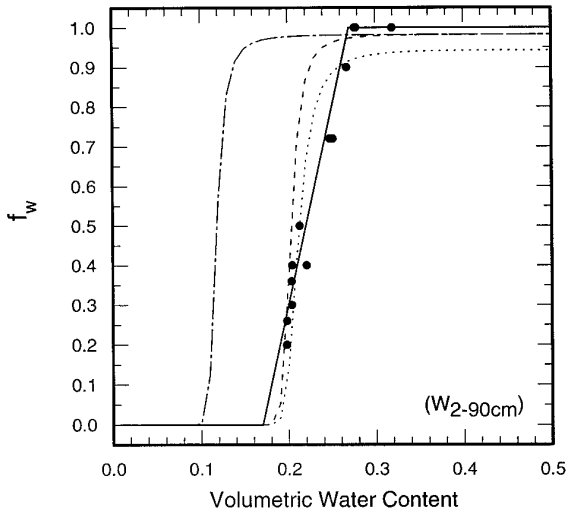

FIG. 8. The soil water stress factor from Fig. 7 and the corresponding average volumetric soil water content in the 2–90-cm-depth interval. Interpolations in time between the profiles shown in Fig. 2 were used as necessary to match the times of the data points in Fig. 7. Rainfall and latent heat data were used to correct obvious water status interpolation errors in two cases. The solid line is an empirical fit to the data, using (A4), characterized by the water content at "incipient water stress" ($W_{isp} = 0.27$) and that at "complete water stress" ($W_{csp} = 0.17$). A multilayered form of this expression (A5) was used in the Tuned version, which resulted in slightly different values of W_{isp} and W_{csp} (Table 1). The broken lines were obtained from the thermodynamic parameterization of water stress [S96, Eq. (C.17)] with different soil texture–dependent parameters. The dash–dot line was generated using the Control version's Ψ_c (from Table 1) and loam soil texture (from Table 2). The dashed line shows Control loam soil texture replaced by the Calibrated version's clay soil texture. The dotted line is the same as the dashed line with Control Ψ_c replaced by Calibrated Ψ_c.

6) generally matched the energy fluxes and the net site CO_2 flux fairly well. This grassland apparently responded quickly to both onset and relief of drought stress. When water stress was severe in August (panels c and d), modeled CO_2 flux tended to be too low in the morning and too high in the afternoon. This same pattern was observed in trial simulations using August data from FIFE86 (Verma et al. 1989). The basis of this pattern is not known, but one possible explanation is the phenomenon known as hydraulic lift (Field and Goulden 1988), which we did not attempt to model.

Substantial seasonal changes in soil respiration (indicated by A_m at night) may also be seen in Fig. 5. This was presumably a function of changes in soil moisture and temperature. Our short-term simulations, using (A7) and observed values for soil moisture and temperature, accurately matched the observed net site CO_2 flux at night. Note that in these simulations both the soil water content and the soil temperature were initialized from field observations and changed insignificantly over the simulation period.

We next turn to the relationship between the apparent level of water stress and soil water status. Using linear interpolation of the Site 16 soil moisture measurements from Fig. 2, we produced 13 detailed soil water profiles (with 11 soil layers each) corresponding in time to each of the 13 empirical estimates of f_w. Each of these 11-layer profiles was recast to the corresponding layers of SiB2 using the $\overline{W}$ function (A9) according to layer thicknesses.

Figure 8 shows the f_w "observations" (solid symbols) plotted against volumetric water content of the the rooting zone (2–90 cm) of SiB2. These data, which span several dry-down and recovery cycles, show a very strong and consistent relationship between the apparent level of physiological drought stress and soil water content.

d. Calibration of the soil in tuned version

After many iterations of seasonlong runs with adjustments to the physiology and soil hydrology, we came to the conclusion that the structure of the soil system in SiB2 was resulting in unrealistic behavior of the soil–plant system, making it difficult to arrive at a satisfactory calibration. For example, the top layer of soil in the model contained no roots. Thus, precipitation entering the soil did not affect the plants until there was sufficient accumulated precipitation to penetrate to the rooting layer, yet with abundant roots near the surface, plants appeared to obtain some water even from light rainfall events. The rooting layer in the Control version of SiB2 (2–90 cm) spans a depth interval with very dynamic variations in moisture content (see Fig. 2), yet as noted above the model only "knows" the average

water content of the entire layer. We found that there could be very large errors in seasonlong simulations of net CO_2 flux—even if W_2 and the canopy water stress parameter were correctly simulated. This was traced to the strong effect of moisture on respiration in the organic-rich soil near the surface. The structure of the soil layers in the Control version of SiB2 (Table 1) were not appropriate to obtain the accurate estimates of moisture and temperature needed by the soil respiration model of Norman et al. (1992). The resulting large errors in soil respiration in seasonlong runs made it difficult to use net CO_2 flux as a diagnostic in the calibration studies.

For these reasons, we modified the Control version of SiB2 with the goal of obtaining a more realistic simulation of the location of water in the soil profile relative to the sinks for water (uptake by roots, direct evaporation from the surface, and drainage) and the physiological elements that respond to water. This is referred to as the Tuned version. This version included the mixed C_3/C_4 canopy submodel noted above, but the most fundamental change in this version was that the canopy could extract water from all three layers of the soil and the depth of these layers was adjusted (Table 1). The canopy water stress factor was thus no longer a property of a single layer of soil, instead it was calculated by weighting the water availability in each soil layer (a local value of f_w) by the density of roots in that layer (A5). For simplicity we used a linear relationship (see Fig. 8) between the water content of each layer and its layer specific f_w (A4). The constants of this equation, W_{isp} and W_{csp}, were assumed to be the same for all layers. To set the root density profile to time-invariant values, it was assumed to be correlated with the soil profile of organic matter. Extraction of water from each layer followed the product of the fractions of available water and roots in each layer (A6). These changes permitted the model to generate more realistic simulations of the soil water during seasonlong runs.

e. Analysis of season-long runs

Figure 9 shows simulations of five output parameters (dotted lines) from three different 142-day runs of SiB2, beginning on DOY 148 and ending on DOY 289, all compared to observations (solid circles). The runs are labeled Control, Calibrated, and Tuned. In the A_m row of panels each simulated day is horizontally compressed so that its normal diurnal cycle (such as in Fig. 4) appears as a vertical trace, where the peak indicates the maximum midday flux of CO_2 uptake, and the nadir indicates the maximum rate of respiratory CO_2 release at night (principally from the soil). The f_w row of panels shows the simulated and observed seasonal course of the water stress factor, and the next three rows of panels show the corresponding moisture content of the soil layers (W_1, W_2, and W_3).

These three runs illustrate some of the complex interactions that occur in seasonlong runs. All runs were started with prognostic initialization values from day 148 observations and were driven by the same precipitation and micrometeorolgical observations. All of the models contained the soil respiration parameterization of Norman et al. (1992), but simulated soil respiration differed from run to run, because of differences in simulated soil moisture and temperature. In the following we will attempt to explain the differences between these simulation results. However, we acknowledge that any ''insights'' gained will be somewhat artificial since they are based partly on modeled behavior.

The Control simulation of A_m shown in Fig. 9 (upper left) match observations very well early in the season, but after day 200, the simulations of A_m at midday are consistently too high (overestimating photosynthesis) and generally underestimate respiration at night (except for ''spikes,'' which follow rainfall events). The Calibrated version tracks the seasonal pattern better than the Control, and the Tuned version is better yet. A noticable difference between the Calibrated and Tuned A_m is the lack of recovery from water stress in the Calibrated version after a major rain event on DOY 217 (which did not penetrate to the root zone, 5–95 cm, of this model version).

Inspection of the second row of panels shows that the soil water stress parameter (f_w) calculated from the prognostic soil moisture was above the observations for most of the season in the Control run, but it matched the observations much better in the Tuned and Calibrated runs. As shown in Fig. 8, the Control soil texture and water stress parameterization were not appropriate for this site. The clay soil at this site holds more water (and a larger fraction of that water is unavailable to plants) than the loam soil specified in the Control. The Tuned and Calibrated runs used water stress parameterizations that were fit to local site observations. However, this is only a partial explanation for the absence of water stress in the Control simulation. As layer 2 dryed down due to the extraction of excessively transpired water, water was ''wicked up'' inappropriately from the third layer (Fig. 9).

Table 4a provides a summary of the simulated hydrologic balance of the three runs. It is interesting how differently the hydrological balance was solved in these runs. For heuristic purposes, we will assume here that the Tuned run is a reasonable approximation of the ''real'' response of the site. Note, however, that there were no direct measurements at Site 16 of infiltration, runoff, or the partitioning of evaporation between canopy and soil, so these model predictions cannot be verified. Over the season, net water loss from the Control soil was 273 mm, whereas the corresponding drawdown of the soil of the Tuned run was only 86 mm. Several factors apparently contributed to this difference of 187 mm. The Control compared to Tuned produced 60 mm less infiltration of precipitation into the soil (P_{W_1}), 37 mm more drainage from the profile (Q_3), 55 mm more

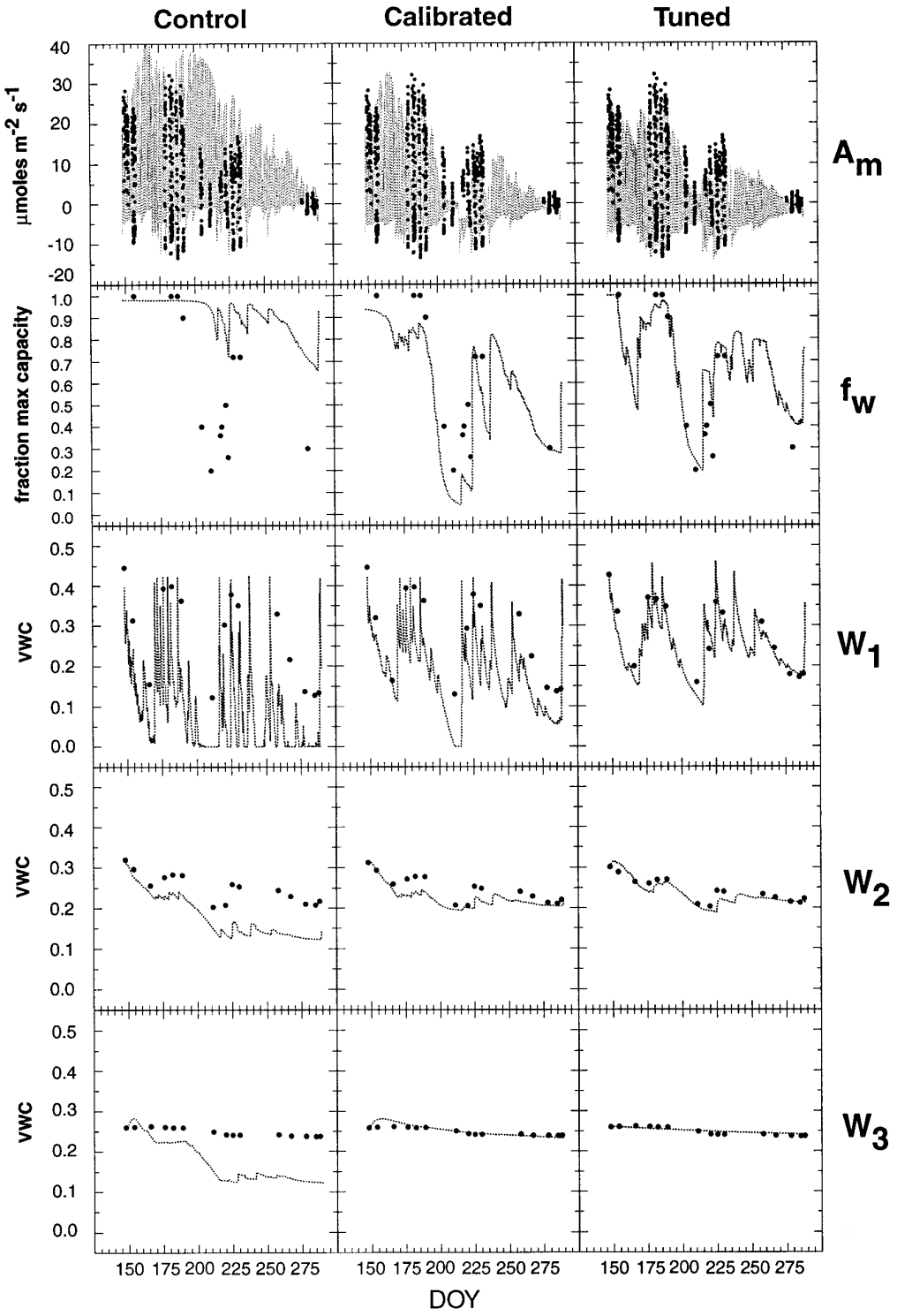

FIG. 9. Continuous long-term SiB2 simulations (dashed lines) of net site CO_2 flux (A_m), soil water stress (f_w), and soil water (W_1, W_2, and W_3) compared to available observations (solid circles) from Site 16, 28 May–16 October 1987 (142 days, DOY 148–289) for the Control, Calibrated, and Tuned versions. Note that at this timescale in the A_m panels diel curves (like those in Fig. 4) are compressed to vertical lines. The f_w observations are from Fig. 7. The soil water observations were processed from Fig. 2 using Eq. (A9).

TABLE 4a. Integration of the hydrological budget for the Control, Calibrated, and Tuned SiB2 runs. The symbols and units are defined in Table A1. All values are in mm. Both runs were for 142 continuous days: 28 May–16 Oct 1987. ΔM is always zero, because total surface standing water was unchanged over the run. Soil gain = (ppt − surface losses) = $P - (E_{ci} + R_{o1} + \Delta M)$. Net soil = (soil gain − soil losses) = $P_{W1} - (E_{ct} + E_{gs} + Q_3)$. E_{ci} is negative when there was more condensation to than evaporation from canopy interception stores. Interlayer flux is negative when net flow was upward. This is not a term in the overall water budget calculations.

		Ppt		Surface losses				Soil gain		Soil losses				Net soil	Interlayer flux	
Run	Version	P	−	E_{ci}	R_{o1}	ΔM	=	P_{W1}	−	E_{ct}	E_{gs}	Q_3	=	ΔW_{soil}	$Q_{1,2}$	$Q_{2,3}$
46	Control	377		24	61	0		292		344	184	37		−273	113	−46
89	Calibrated	377		28	82	0		267		221	151	0		−104	123	−11
45	Tuned	377		−6	31	0		352		308	129	0		−86	109	−7

evaporation from the soil (E_{gs}), and 36 mm more transpiration extracted by the canopy (E_{ct}). We had anticipated that the canopy transpiration would be in error, because the soil and water stress parameterizations were not calibrated to the site, but it is apparent that this was only one of several problems in the Control simulation of this system.

The net water balance of the Calibrated version was much closer to the Tuned. It lost only 18 mm more water over the season. However, this balance was achieved somewhat differently than in the Tuned run: 85 mm less water infiltrated the soil, but this was offset by canopy transpiration being 87 mm lower, and direct soil evaporation being 22 mm higher. One notable difference between the Calibrated and the Control run is in the amount of direct soil evaporation. An improved soil evaporation parameterization developed from process-level studies at FIFE by S92b reduced E_{gs} from 184 to 151 mm.

The larger runoff from the Calibrated run relative to the Control is related to the lower saturated conductivity (K_s) of a clay soil compared to a loam (Table 2). Empirical studies of the soil water balance (section 2h) were not compatible with such a large runoff. We did not attempt to correct this in the Calibrated version, but we did in the Tuned version. To get more water to infiltrate into the soil of the Tuned version (which also had a clay soil), we experimented with increasing K_s. However, this had the undesirable side effect of inappropriately increasing unsaturated flow between layers. To avoid this we introduced a separate constant (K_{infil}) that applied only when there was free water in the above-ground "puddle" (M_g). We choose a value for K_{infil} about 10 times larger than K_s. This implies that the infiltration capacity for the field soil should, in fact, be different than the saturated flow of a homogeneous soil column. One possible rationalization is that there are "conduits" for free water in the soil structure such as those produced by roots, gopher and ant holes, or cracks (Germann and Beven 1985). We also arbitrarily reduced direct evaporation of precipitation from the canopy (E_{ci}) by making the interception capacity ($M_{c_{max}}$) smaller, causing a larger fraction of precipitation to drip off from M_c to M_g.

The near absence of water stress in the Control run caused it to transpire the largest total quantity of water (Table 4a). It also had correspondingly higher gross photosynthesis (Table 4b). At a finer level, photosynthesis and transpiration of the Tuned run were greater than the Calibrated run. This was partly due to differences in the soil parameterization that permitted 85 mm more water to infiltrate into the soil over the course of the Tuned run. Both runs appear to have similar levels of water stress (Fig. 9, f_w), but overall stress was slightly higher in the calibrated version. Water use efficiency (WUE) calculated on the basis of net photosynthesis was similar in all versions. For the C_4 component, WUE = 5.56–6.02 mmol CO_2 per mol H_2O. For the C_3 component (only in the Tuned version), WUE = 3.73. These compared to 7 and 3 mmol CO_2 per mol H_2O expected for C_4 and C_3 species respectively (Berry and Downton 1982). The presence of C_3 species in the Tuned version decreased its WUE relative to the Control and Calibrated runs.

Net ecosystem carbon balance (A_m) of these runs is remarkably different (Table 4b). The Tuned run resulted in a slight net accumulation of carbon over the course of the run of 53 gC m^{-2}. The Calibrated run accumulated about 3.4 fold more and the Control run 18.2 fold more

TABLE 4b. Integration of CO_2 fluxes and water use efficiency for the Control, Calibrated, and Tuned SiB2 runs. Symbols and units are defined in Table A1. All CO_2 flux values are in gC m^{-2}. Water use efficiency (WUE) units are [(mmol CO_2) (mol $H_2O)^{-1}$]. All runs were for 142 continuous days; 28 May–16 Oct 1987. Dashes mean not applicable. The mathematical relationships between the symbols are defined (A1–A3).

		C_3 component			C_4 component			Canopy totals			Soil	Site	WUE		
Run	Version	A_3	R_{D3}	A_{c3}	A_4	R_{D4}	A_{c4}	A	R_D	A_c	R_{soil}	A_m	A_{c3}/E_{ct3}	A_{c4}/E_{ct4}	A_c/E_{ct}
46	Control	—	—	—	1347	48	1299	1347	48	1299	341	958	—	5.68	5.68
89	Calibrated	—	—	—	912	30	882	912	30	882	705	177	—	6.02	6.02
45	Tuned	355	64	291	796	109	687	1151	173	978	925	53	3.73	5.56	4.76

carbon over the season. These differences stem largely from the simulation of soil respiration (R_{soil}). Gross soil respiration in the Control run was less than half of that in the Tuned run. Yet, the same soil respiration parameterization was used in each model run. Inspection of the model output showed that this was occurring because the simulated water content at 10 cm (W_{10cm}) required by the process model of Norman et al. (1992) was not realistic in the Control run. Note that W_{10cm} was not explicitly simulated by SiB2. Instead it was obtained by weighted interpolation of the SiB2 soil water profile (W_1, W_2, and W_3) using (A9). To address these errors we modified the Tuned version to have a more realistic treatment of the soil profile with layers of 0–15 cm, 15–90 cm, and 90–140 cm, and the model was changed to permit the canopy to extract water from all layers of the soil depending on the root density and water availability of the layers. As shown in Fig. 9, the Tuned version reproduced the soil water content of all three layers very accurately. The prediction of W_1 was greatly improved by allowing D_1 to be thicker than the Control version, resulting in an improved estimation of W_{10cm} and consequently R_{soil}. This is illustrated by the values of A_m at night closely matching observations throughout the season. In SiB2 canopy respiration (R_D) represents only leaf dark respiration (typically 2%–3% of V_{max0}). SiB2 currently has no method of calculating canopy maintainence or growth respiration; R_D was 4–5 times higher in the Tuned version compared to Control and Calibrated. This was a direct result of the higher value of the Tuned dark respiration rate parameter (R_d) as fit to local leaf-level measurements. It is possible that unaccounted canopy respiration quantities in the Control and Calibrated versions, which used a standard value of R_d, are somehow reflected in the higher Tuned R_d, but we have no way to evaluate this. These problems illustrate the importance of accurate prediction of site respiration as well as photosynthesis.

f. Statistical analysis of the simulation results

To provide a more quantitative basis for the analysis of different version runs, we turned to a statistical approach. Figure 10 shows "one-to-one" plots of eight output variables (y axis) compared to corresponding observations (x axis) for the Tuned version. Table 5 presents the data for three statistical indices SEE, NSEE, and BIAS (defined in section 2e). We have used these indices to assess the match of paired simulations and observations for the Control, Calibrated, and Tuned runs. The BIAS statistic indicated any systematic bias in the relationship between simulations and observations. For example, there is visible bias in the plot of Tuned H_m (Fig. 10), which has a regression slope of 1.42 (Table 5). The scatter about the one-to-one line is indicated by the SEE statistic. For example, Tuned A_m, which has a BIAS of 1.00 (no bias), does have significant scatter with an SEE of 4 μmol m^{-2} s^{-1}. The NSEE statistic indicates the relative errors in these estimates. For example, Tuned A_m has an NSEE of 30%, while Tuned H_m has an NSEE of 62%, indicating (relative to its own scale) that A_m was simulated more accurately than H_m.

Bar charts of the NSEE statistic illustrate the relative accuracies of the Tuned, Calibrated, and Control simulations (Fig. 11). Reported uncertainties in flux measurements are indicated by horizontal dashed lines. This is intended as a nonrigorous statistical technique to evaluate model deviations compared to observational uncertainties. An analogous technique is discussed in Baldocchi (1992).

In this work net CO_2 flux (A_m) was used as the primary diagnostic for calibration and tuning of the model, and large improvements were realized in the accuracy of A_m simulation as shown in Fig. 11. Latent heat flux, soil water, and to a lesser extent, sensible heat flux estimates were also improved as A_m was calibrated. Net radiation (R_n) and upwelling longwave ($L\uparrow$) matched very well to the observations and were not affected by the changes that improved A_m. The improvement of the upwelling solar radiation ($S\uparrow$) in the Tuned version resulted from adjustments to the model leaf reflectances and transmittances (Table 1) guided by Site 16 observations of canopy solar reflectance and transmittance. However, since R_n was unaffected, we presume the improvement in $S\uparrow$ was inconsequential.

4. Conclusions

The experiments reported here have examined SiB2's ability to predict changes in temperature, hydrologic state, energy flux, and CO_2 flux over the 1987 growing season at FIFE Site 16. The results reported here demonstrate that SiB2, when properly calibrated to this site, can accurately simulate the observed responses of this ecosystem, during the growing season, forced only by an above-canopy atmosphere and a prescribed canopy phenology. In this model, stomatal regulation, which controls transpiration and energy partitioning, is linked to photosynthesis, a process that is universal and mechanistically well understood. Another advantage of basing the parameterization used in SiB2 on photosynthesis is that it can, in theory, be calibrated from leaf-scale measurements of photosynthesis and stomatal conductance. Indeed, the calibration used for general simulation of C_4–grasslands in the CSU GCM is based on studies with leaves of *Zea mays*. In the present study, we compared two independent ways to fit C_4–V_{max0}, the major adjustable parameter of the photosynthesis model. First, we analyzed published measurements of gas exchange of individual leaves of the dominant species at FIFE. Second, we fit this parameter by tuning the canopy model to fit the observed net CO_2 flux measured by eddy correlation above the grassland. These estimates agreed well with each other and were quite similar to the general calibration used for this ecosystem in the GCM.

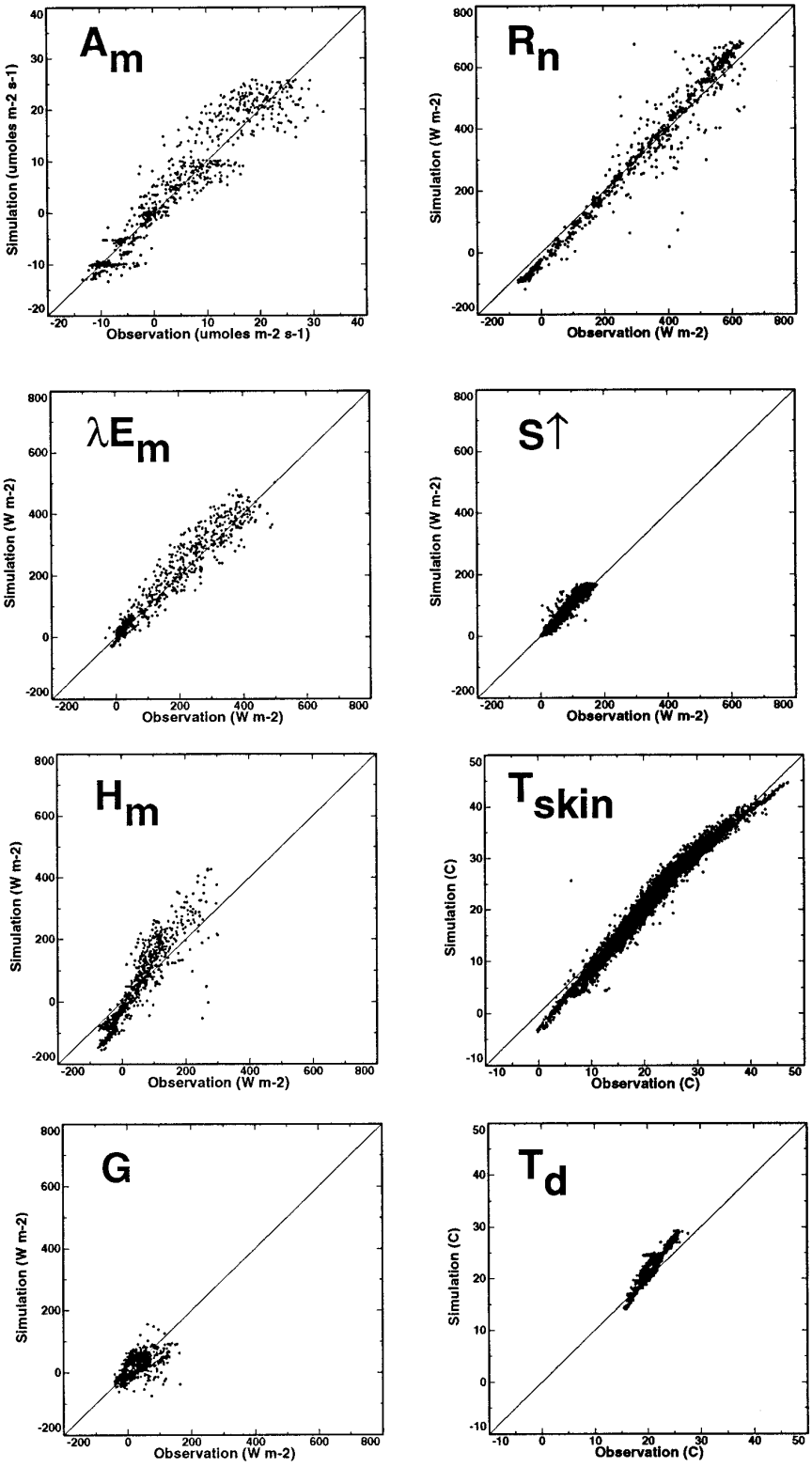
Am
Simulation (umoles m-2 s-1)
Observation (umoles m-2 s-1)
Rn
Simulation (W m-2)
Observation (W m-2)
λEm
Simulation (W m-2)
Observation (W m-2)
S↑
Simulation (W m-2)
Observation (W m-2)
Hm
Simulation (W m-2)
Observation (W m-2)
Tskin
Simulation (C)
Observation (C)
G
Simulation (W m-2)
Observation (W m-2)
Td
Simulation (C)
Observation (C)

TABLE 5. Simulation versus observation statistics for Control, Calibrated Control, and Tuned SiB2 runs. The symbols and units are defined in Table A1. Each of the runs was for 142 continuous days: 28 May–16 October 1987. NSEE is given as a percent.

SiB2 output parameter	Source of observations	n	Control (run 46)			Calibrated (run 89)			Tuned (run 45)		
			SEE	NSEE	BIAS	SEE	NSEE	BIAS	SEE	NSEE	BIAS
A_m	Site 16 eddy flux sta, A_m	806	11	95	0.97	5	41	0.91	4	30	1.00
f_w	(Fig. 9)[a]	13	0.5	69	0.05	0.20	28	1.08	0.15	21	0.74
R_n	Site 16 eddy flux sta, R_n	913	51	15	1.07	53	15	1.05	52	15	1.10
λE_m	Site 16 eddy flux sta, λE_m	813	78	39	1.12	54	26	0.89	39	18	1.03
H_m	Site 16 eddy flux sta, H_m	847	70	74	0.95	58	62	1.39	59	62	1.42
G	Site 16 eddy flux sta, G	927	34	70	0.74	38	80	1.02	32	67	0.55
W_1	(Fig. 3)[b]	15	0.18	57	0.94	0.10	32	1.01	0.04	13	1.01
W_2	"	15	0.06	24	1.83	0.03	10	0.92	0.02	6	1.11
W_3	"	15	0.08	30	6.39	0.01	3	1.52	0.01	2	0.61
T_g	Site 16 eddy flux sta, T_{0-5cm}	937	2.7	11	0.74	2.4	10	0.78	2.2	9	0.80
T_g	FIFE met-sta avgs, T_{10cm}	6617	2.0	9	0.83	2.0	9	0.87	1.8	8	0.95
T_d	FIFE met-sta avgs, T_{50cm}	6544	1.2	6	1.31	2.1	10	1.37	1.9	9	1.42
T_{skin}	FIFE met-sta avgs, T_{skin}	6720	1.7	7	0.98	1.2	5	1.05	1.6	7	1.10
$S\uparrow$	FIFE met-sta avgs, $S\uparrow$	6749	35	37	1.29	35	37	1.29	14	15	1.08
$L\uparrow$	FIFE met-sta avgs [Eq. (8)][c]	6720	10	2	0.95	7	2	1.04	9	2	1.09

[a] Soil water stress was estimated for each of 13 different days by fitting simulated fluxes to observed eddy station fluxes using adjustments to f_w until error was minimized.

[b] For each of 15 different days the soil water profile was averaged over different depth intervals (Table 1).

[c] $L\uparrow$ was not measured directly at the FIFE met-stations. T_{skin} was converted to $L\uparrow$.

We note that this may be fortuitous, and that this agreement does depend on knowledge of the canopy integration factor (calculated from the leaf area index) and soil respiration. Nevertheless, this study lends support to this calibration scheme.

The present study provided an excellent opportunity to test SiB2's ability to model seasonal changes in soil moisture stress. During the season, as photosynthetic activity went up and down through several drying cycles, there was a direct correspondence between photosynthetic activity and soil water content, with maximum soil water stress evident during yeardays 200–225 (Fig. 9, Tuned). When the model correctly simulated changes in CO_2 flux associated with drought stress, it also corectly simulated the corresponding changes in latent and sensible heat fluxes. These results illustrate that net CO_2 flux is a very sensitive diagnostic of the physiological processes that control surface energy exchange.

The mechanisms of water stress effects are still an active area of research (Sharkey and Badger 1982; Kaiser 1987; Bjorkman 1989; Chaves 1991; Quick et al. 1992; Pereira and Chaves 1993). The phyto–hormone abscisic acid (ABA) is most likely involved (Johnson et al. 1991; Tardieu et al. 1991, 1993; Tardieu and Davies 1993a,b). We should note that modelers differ on whether to use soil moisture or leaf water potential as the key state variable, and whether this has a *direct* or an *indirect* effect on stomatal conductance. Earlier versions of SiB calculated water stress through leaf water potential (LWP), as a function of soil water potential and the rate of transpiration (Sellers et al. 1986). In SiB2 the calculation of LWP was eliminated. In this study we found canopy water stress could be adequately predicted from soil water content or soil water potential, and by assuming that stomatal conductance was *indirectly* affected by water stress through its effect on photosynthesis. Other modeling studies have addressed water stress at FIFE. Hope (1992) and Gao (1994) used a *direct* effect of water stress on stomatal conductance, while Chen and Coughenour (1994) used a method similar to ours. However, neither of these studies specifically calibrated their models for water stress, and their simulations do not appear to reproduce the episodes of water stress at this site. Modeling studies by Kim and Verma (1991b), Kim and Verma (1991a), and Kim et al. (1992) specifically address water stress at this site and show that alternative formulations can be made to work equally well. All of the above studies used observed soil moisture content as an input parameter. Our study differs in that we predict soil water content and the level of water stress.

This study identified some areas of concern. Sparse and noisy data on leaf area index (LAI) are a significant source of concern in this study, and continue to be, as we extend this work into the years 1988–89. We estimate

←

FIG. 10. One-to-one plots of Tuned version simulations (y axis) against available observations (x axis) for net site CO_2 flux (A_m), net radiation (R_n), latent heat (λE_m), upwelling shortwave radiation ($S\uparrow$), sensible heat (H_m), site skin temperature (T_{skin}), soil heat (G), and deep soil temperature (T_d). These data are from the same Tuned run as in Fig. 9. The statistics corresponding to these one-to-one plots are listed in Table 5.

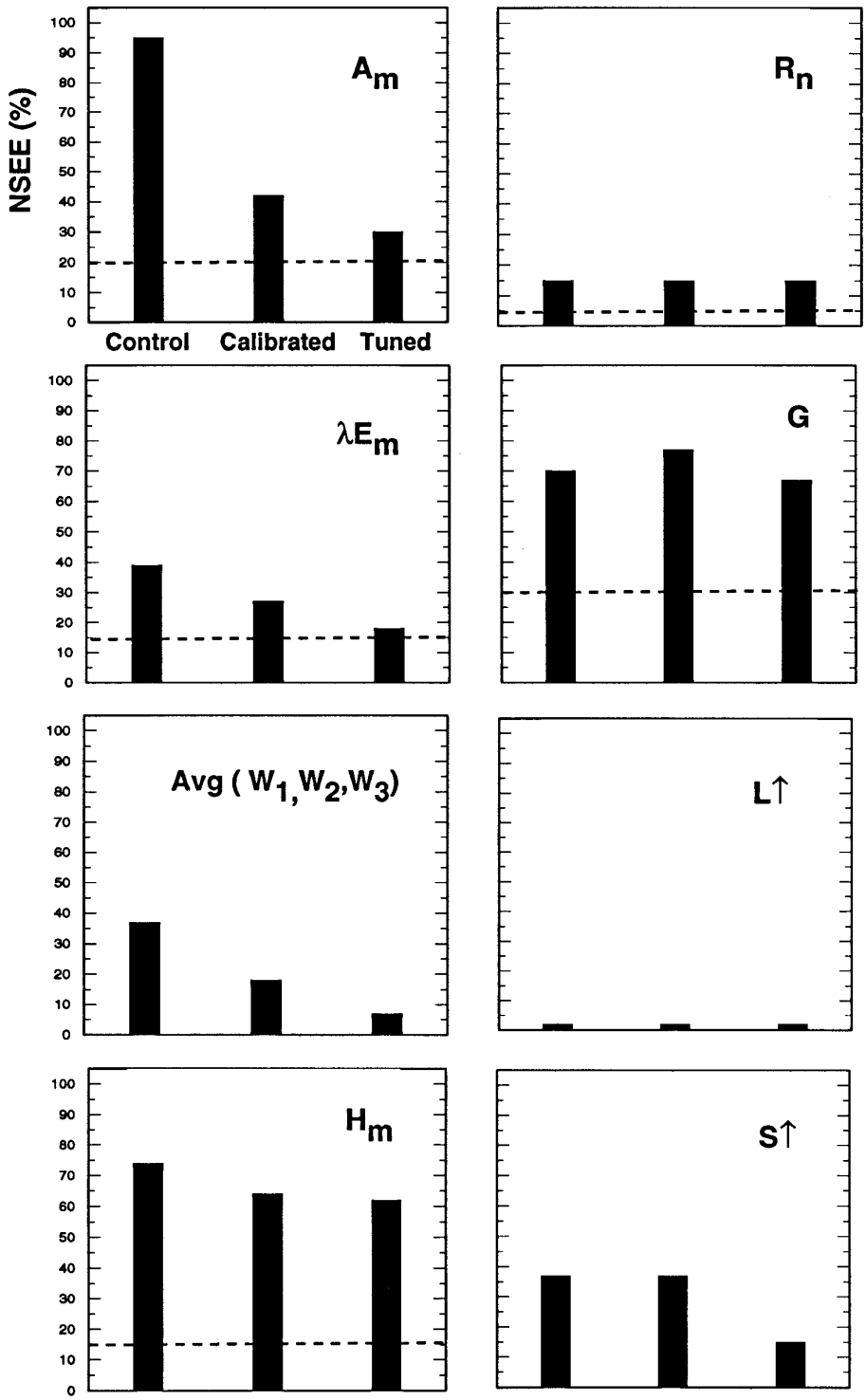

FIG. 11. Bar graphs of the NSEE statistic for the Control, Calibrated, and Tuned versions: net site CO_2 flux (A_m), net radiation (R_n), latent heat (λE_m), soil heat (G), soil water (as an average of the NSEE's for W_1, W_2, and W_3), upwelling longwave radiation ($L\uparrow$), sensible heat (H_m), and upwelling shortwave radiation ($S\uparrow$). These data are from the same runs as in Fig. 9. The NSEE values used in these plots were taken directly from Table 5. Each horizontal dashed line indicates the ±% overall uncertainty assigned by FIFE investigators to that flux measurement (Sellers et al. 1990, 4–22).

that simulations of site respiration were the largest source of error in our site CO_2 flux modeling. Soil respiration estimation [Eq. (A7)] requires accurate prediction of soil temperature and moisture [note that Kim et al. (1992), Gao (1994), and Chen and Coughenour (1994) avoided this problem by supplying observed 10-cm values]. In our simulations, soil moisture was predicted as output of the model, and respiration was accurately predicted only when soil conditions were correctly simulated. This required a more realistic representation of the profile of roots, moisture, and temperature in the soil. Error analysis revealed a substantial bias in our simulations of H_m (Figs. 10 and 11). Other investigators have discussed problems at FIFE in the context of modeling H_m from a SVATS or remotely sensed T_{skin} (Vining and Blad 1992; Hall et al. 1992; Cooper et al. 1995), suggesting that the coupling of different surface thermal radiators (e.g., litter, bare soil, rocks, or sun and shade leaves) to aerodynamic conductances is a likely source of error.

The result that SiB2 does an adequate job of simulating the seasonal course of energy, water, and CO_2 exchange at a single well-characterized site provides a rigorous test of the way that the biophysical and physiological mechanisms controlling these processes are represented in SiB2. We suggest that this is a fundamental requirement for simulation of these processes at the scale of a GCM. However, we acknowledge that scale-dependent problems (e.g., aggregation of subgrid-cell processes, and averaging of nonlinear properties) must also be considered in extrapolating from these local-scale calibration studies to the scale of a GCM grid box.

Acknowledgments. We note the passing of our friend and colleague, Dr. Cyril Grivet, who was among those lost in the tragic crash of TWA flight 800 the evening of 17 July 1996. Cyril's way with instruments, his gift for mathematics, and his generosity are missed. This research was supported by NASA under Grants NAGW-3699 (FIFE) and NAS 531731 (EOS). We are particularly grateful to Alan Betts for the FIFE sitewide average meteorology dataset; to Shashi Verma for the site 16 eddy flux dataset; to the staff of FIFE who assembled the FIFE CD-ROM; and to Jim Collatz, Scott Denning, and Dave Randall for sharing their wisdom.

APPENDIX

Description of Differences from the Standard SiB2 Model

A copy of version 1.0 of standard SiB2 (SiB2v1.0) FORTRAN source code and documentation can be obtained from J. Collatz (Code 923, Goddard Space Flight Center/NASA, Greenbelt, MD 20771). Copies of the current study's modified SiB2v1.0 source code and accompanying sets for a Unix workstation with a FORTRAN compiler can be obtained from author J. Berry. Figure A1 presents a schematic diagram of the structure and key parameters of what we call our Tuned version of SiB2 (Fig. 1); see Table A1 for definition of symbols. The differences from SiB2v1.0 are described below.

a. Mixed C_3/C_4 canopy

SiB2v1.0 is structured to produce bulk values of leaf respiration (R_D), net photosynthesis (A_c), and stomatal conductance (g_c) for either a C_3 or C_4 canopy, but not for a mixed canopy [S96, Eqs. (C.22)–(C.24)]. Equations (A1)–(A3) below are presented as a simple enhancement to the above equation set to emulate a mixed C_3/C_4 canopy like that present at Site 16. The two types are treated as separate units within the SiB2 resistor network analog (Fig. A1). Both types share a common leaf temperature (T_c) and leaf surface humidity (e_s), which assumes that the two photosynthetic types form a homogenous mixture and share a single set of energy budget and humidity resultants. (This would not be appropriate if the canopy were composed of C_3 or C_4 clumps large enough to generate different microclimates.) Individual values of leaf surface CO_2 concentration (c_{s3}, c_{s4}), stomatal conductance (g_3, g_4), intercellular CO_2 concentration (c_{i3}, c_{i4}), leaf dark respiration (R_{D3}, R_{D4}), photosynthetic CO_2 uptake (A_3, A_4), land canopy net CO_2 flux (A_{c3}, A_{c4}) are calculated within the photosynthetic submodel. In practice, we do two calculations, one for each photosynthetic type as described in S96. These provisional results (R'_D, A', A'_c, g'_c) are then scaled according to the observed fractional abundances of each photosynthetic type (f_{c3}, f_{c4}; where $f_{c3} + f_{c4} = 1$) and summed to produce bulk canopy values:

$$X_n = f_n X'_n \tag{A1}$$

$$X = X_3 + X_4, \tag{A2}$$

where X may be R_D, A, A_c, or g_c; n may be 3 and 4; the prime indicates the respective value for a 100% C_3 or C_4 canopy; the units of R_D, A, and A_c are μmol m^{-2} s^{-1}; and the units of g_c are mol m^{-2} s^{-1}. Equation (A2) redefines R_D, A_c, and g_c, respectively from S96 [Eqs. (C.22)–(24)]. The energy balance is solved using a time-stepped, bulk canopy g_c, and latent heat ($\lambda E_{ct} = \lambda E_{ct3} + \lambda E_{ct4}$) and corresponding transpiration flux ($E_{ct} = E_{ct3} + E_{ct4}$) are partitioned according to g_n/g_c.

Net site CO_2 flux (A_m) is defined as

$$A_m = A_c - R_{soil} = A - R_D - R_{soil}, \tag{A3}$$

where R_{soil} is the soil respiration rate [Eq. (A7)].

b. Water stress parameterization

In SiB2v1.0 the impact of drought stress on leaf physiology is controlled by an inhibition factor, f_w, which varies between 1.0 (no stress) and 0.0 (complete stress). This factor attenuates the operational value of V_{max} from

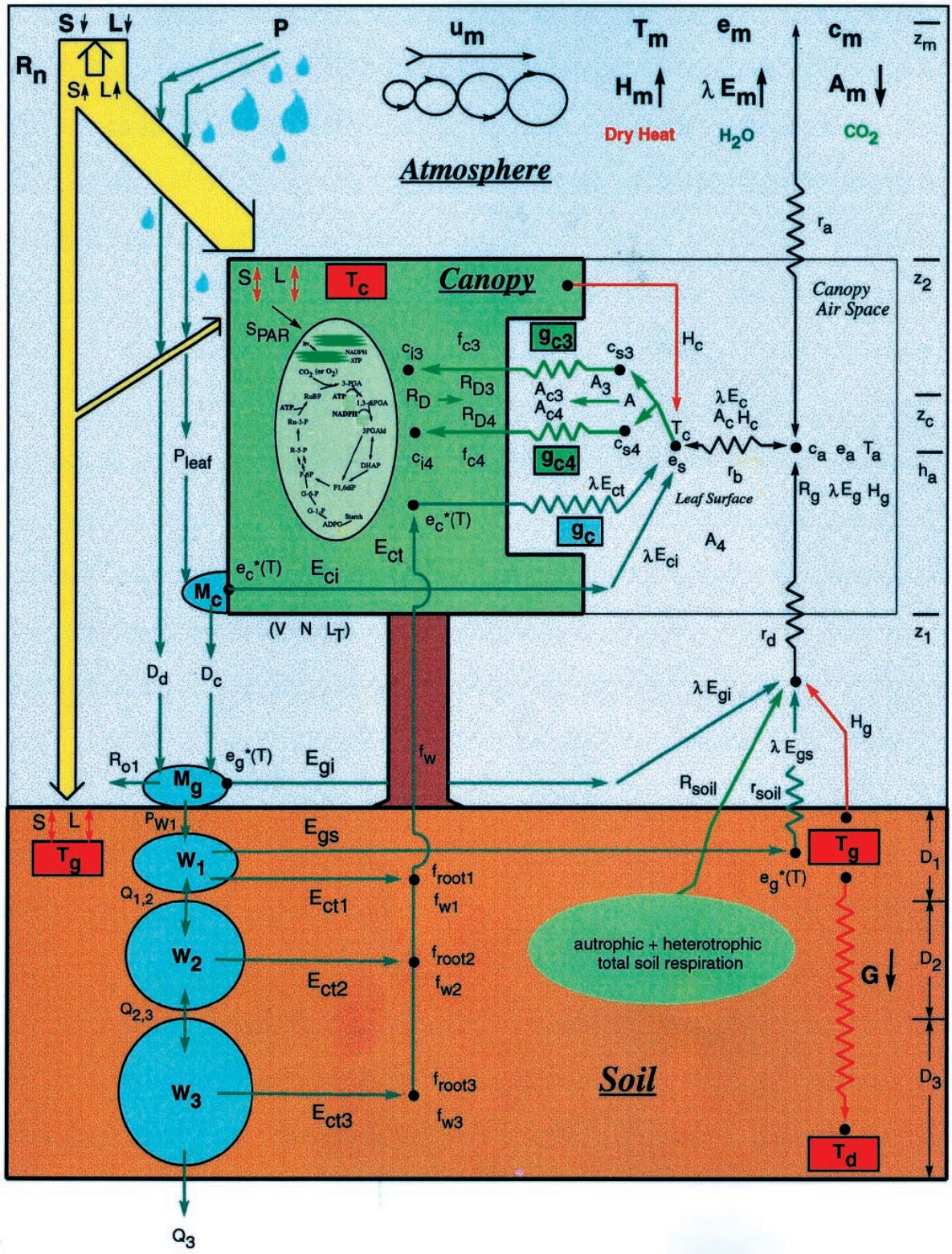
S↓ L↓
P
u_m
T_m
e_m
c_m
z_m
R_n
S↑ L↑
H_m↑
λE_m↑
A_m↓
Dry Heat
H_2O
CO_2
Atmosphere
r_a
S L
T_c
Canopy
Canopy Air Space
z_2
S_{PAR}
g_{c3}
c_{i3}
f_{c3}
c_{s3}
H_c
R_{D3}
A_{c3}
A_3
R_D
A
λE_c
$A_c H_c$
z_c
R_{D4}
A_{c4}
T_c
P_{leaf}
c_{i4}
f_{c4}
g_{c4}
c_{s4}
c_a e_a T_a
h_a
e_s
r_b
λE_{ct}
R_g λE_g H_g
Leaf Surface
$e_c^*(T)$
g_c
A_4
E_{ct}
λE_{ci}
$e_c^*(T)$
E_{ci}
M_c
(V N L_T)
r_d
z_1
D_d
D_c
λE_{gi}
H_g
R_{o1}
$e_g^*(T)$
E_{gi}
f_w
λE_{gs}
R_{soil}
r_{soil}
M_g
S L
P_{W1}
E_{gs}
T_g
W_1
f_{root1}
$e_g^*(T)$
T_g
D_1
$Q_{1,2}$
E_{ct1}
f_{w1}
autrophic + heterotrophic
total soil respiration
W_2
f_{root2}
D_2
G
E_{ct2}
f_{w2}
$Q_{2,3}$
W_3
f_{root3}
Soil
D_3
E_{ct3}
f_{w3}
T_d
Q_3

TABLE A1. Notation.

Symbol	Definition	Units
A	Canopy bulk gross photosynthesis [CO_2 flux, see Eq. (A2c)]	μmol m^{-2} s^{-1}
A_3	Canopy C_3 fraction gross photosynthesis (CO_2 flux)	μmol m^{-2} s^{-1}
A_4	Canopy C_4 fraction gross photosynthesis (CO_2 flux)	μmol m^{-2} s^{-1}
A_3'	Gross photosynthesis for a 100% C_3 Canopy (CO_2 flux)	μmol m^{-2} s^{-1}
A_4'	Gross photosynthesis for a 100% C_4 Canopy (CO_2 flux)	μmol m^{-2} s^{-1}
A_c	Canopy bulk net photosynthesis [CO_2 flux, see Eq. (A2f)]	μmol m^{-2} s^{-1}
A_{c3}	Canopy C_3 fraction net photosynthesis (CO_2 flux)	μmol m^{-2} s^{-1}
A_{c4}	Canopy C_4 fraction net photosynthesis (CO_2 flux)	μmol m^{-2} s^{-1}
A_m	Above canopy (meas ht) net site CO_2 flux [see Eq. (A4)]	μmol m^{-2} s^{-1}
a_{rsoil}	Soil evaporative resistance regression constant 1	—
a_{Rsoil}	Soil respiration scaling factor	—
a_{sN}	Reflectance fraction, NIR, soil surface	—
a_{sV}	Reflectance fraction, PAR, soil surface	—
b	Stomatal conductance intercept	mol m^{-2} s^{-1}
B	Hydraulic power term, all soil layers	—
B_1	Hydraulic power term, soil layer 1	—
B_2	Hydraulic power term, soil layer 2	—
B_3	Hydraulic power term, soil layer 3	—
b_{rsoil}	Soil evaporative resistance regression constant 2	—
C_1	R_b coefficient	—
C_2	R_d coefficient	—
c_a	Canopy air CO_2 concentration	Pa
c_{i3}	Canopy C_3 leaf intercellular CO_2 concentration	Pa
c_{i4}	Canopy C_4 leaf intercellular CO_2 concentration	Pa
c_m	Above canopy (measurement height) CO_2 concentration	Pa
c_{s3}	Canopy C_3 leaf surface CO_2 concentration	Pa
c_{s4}	Canopy C_4 leaf surface CO_2 concentration	Pa
$C_{soilfac}$	Soil thermal properties scaling factor	—
d	Canopy zero plane displacement	m
D_1	Thickness, soil layer 1	m
D_2	Thickness, soil layer 2	m
D_3	Thickness, soil layer 3	m
D_c	Quantity of intercepted water dripping from canopy	m
D_d	Quantity of precipitation falling through canopy gaps	m
DOY	Sequential day of the year	days
D_r	Rooting depth ($D_1 + D_2$)	m
D_T	Soil depth ($D_1 + D_2 + D_3$)	m
e_a	Canopy air vapor pressure	mb
$e_c^*(T)$	Canopy temperature saturated vapor pressure	mb
E_c	Quantity of water lost from site due to time-integrated λE_c	kg m^{-2}
E_{ci}	Quantity of water lost from site due to time-integrated λE_{ci}	kg m^{-2}
E_{ct}	Quantity of water lost from site due to time-integrated λE_{ct}	kg m^{-2}
E_{ct3}	Quantity of water lost from site due to time-integrated λE_{ct3}	kg m^{-2}
E_{ct4}	Quantity of water lost from site due to time-integrated λE_{ct4}	kg m^{-2}
E_g	Quantity of water lost from site due to time-integrated λE_g	kg m^{-2}
E_{gi}	Quantity of water lost from site due to time-integrated λE_{gi}	kg m^{-2}
E_{gs}	Quantity of water lost from site due to time-integrated λE_{gs}	kg m^{-2}
$e_g^*(T)$	Ground surface temperature saturated vapor pressure	mb
e_m	Above canopy (measurement height) vapor pressure	mb
e_s	Canopy leaf surface vapor pressure	Pa
f	C_4 fraction of absorbed quanta used for RuBP	mol CO_2 mol^{-1} quanta
f_{c3}	Fraction of the canopy that is C_3 species	—
f_{c4}	Fraction of the canopy that is C_4 species	—
f_d	Leaf respiration as fraction of V_{max0} (R_d/V_{max0})	—

←

FIG. A1. A schematic diagram of the Tuned version of SiB2. The symbols and units are defined in Table A1. Across the top of the diagram are the SiB2 micrometeorological driving parameters and the resulting net fluxes of radiation, sensible heat, water, and CO_2 shown in yellow, red, blue, and green, respectively. The insert in the center of the canopy depicts the biochemical transformations that occur in a chloroplast. The photosynthesis model does not explicitly predict all of these reactions, but it does predict the steady-state limitations of the overall process. *Note added in proof*: Inside the box rules for *Canopy Air Space* the symbols $\mathbf{A}_3$ and $\mathbf{A}_4$ should be omitted.

TABLE A1. (*Continued*)

Symbol	Definition	Units
f_{root1}	Functional root fraction, soil layer 1	—
f_{root2}	Functional root fraction, soil layer 2	—
f_{root3}	Functional root fraction, soil layer 3	—
f_w	Canopy soil water stress inhibition, aggregate factor	—
f_{w1}	Canopy soil water stress inhibition due to soil layer 1	—
f_{w2}	Canopy soil water stress inhibition due to soil layer 2	—
f_{w3}	Canopy soil water stress inhibition due to soil layer 3	—
G	Net site soil heat flux	W m^{-2}
G_1	Aerodynamic kinetic factor	—
G_2	Aerodynamic momentum factor	—
G_3	Aerodynamic heat transfer factor	—
G_4	Aerodynamic transition layer factor	—
g_a	Canopy air to above canopy air aerodynamic conductance	mol m^{-2} s^{-1}
g_b	Canopy leaves boundary layer aerodynamic conductance	mol m^{-2} s^{-1}
g_c	Canopy bulk stomatal conductance [see Eq. (A3c)]	mol m^{-2} s^{-1}
g_{c3}	Canopy C_3 fraction stomatal conductance	mol m^{-2} s^{-1}
g_{c4}	Canopy C_4 fraction stomatal conductance	mol m^{-2} s^{-1}
g'_{c3}	Stomatal conductance for a 100% C_3 canopy	mol m^{-2} s^{-1}
g'_{c4}	Stomatal conductance for a 100% C_4 canopy	mol m^{-2} s^{-1}
g_d	Below canopy air to canopy air aerodynamic conductance	mol m^{-2} s^{-1}
$G(\overline{\mu})$	Relative leaf area projected in direction $\overline{\mu}$	—
h_a	Canopy source height for heat	m
H_c	Canopy sensible heat flux	W m^{-2}
H_g	Ground sensible heat flux	W m^{-2}
H_m	Above canopy (measurement height) net site sensible heat flux	W m^{-2}
h_{soil}	Relative humidity of the soil pore space	—
k	Mean canopy extinction coefficient	—
k_g	Stomatal opening/closing time constant	s^{-1}
K_{infil}	Maximum soil infiltration conductivity	m s^{-1}
K_s	Hydraulic conductivity at sat, all soil layers	m s^{-1}
K_{s1}	Hydraulic conductivity at sat, soil layer 1	m s^{-1}
K_{s2}	Hydraulic conductivity at sat, soil layer 2	m s^{-1}
K_{s3}	Hydraulic conductivity at sat, soil layer 3	m s^{-1}
$L\uparrow$	Site upward longwave radiation	W m^{-2}
$L\downarrow$	Downward longwave radiation (S96: $F_{\Gamma,d(0)}$)	W m^{-2}
L_G	Canopy leaf area index, green fraction ($L_T N$)	—
l_l	Canopy leaf length	m
l_w	Canopy leaf width	m
L_T	Canopy leaf area index, total	—
m	Stomatal conductance slope	—
M_{cw}	Water intercepted on the canopy	m
$M_{c_{\max}}$	Canopy maximum interception factor	m
M_{cs}	Snow and ice intercepted on the canopy	m
$M_{g_{\max}}$	Ground maximum interception factor	m
M_{gs}	Snow and ice intercepted on the ground surface	m
M_{gw}	Water intercepted on the ground surface	m
N	Fraction of the canopy that is green	—
NIR	Near-infrared radiation	—
P	Above canopy precipitation	μm s^{-1}
PAR	Photosynthetically active radiation (visible)	—
P_{leaf}	Quantity of precipitation hitting canopy	m
P_{W1}	Quantity of water infiltrating into soil layer 1 (from W_1)	m
Q	Absorbed quantum flux	μmol m^{-2} s^{-1}
$Q_{1,2}$	Net movement of water from soil layer 1 to 2	m
$Q_{2,3}$	Net movement of water from soil layer 2 to 3	m
Q_3	Quantity of water lost from site due to soil layer 3 drainage	m
r_a	Canopy air to above canopy air aerodynamic resistance	s m^{-1}
r_b	Canopy leaves boundary layer aerodynamic resistance	s m^{-1}
RB1	Nonneutral condition aerodynamic correction factor	—
RB2	Neutral conditions aerodynamic correction factor	—
r_d	Below canopy air to canopy air aerodynamic resistance	s m^{-1}
R_d	Rate dark respiration (at 25°C)	μmol m^{-2} s^{-1}
R_D	Canopy bulk leaf respiration (CO_2 flux)	μmol m^{-2} s^{-1}
R_{D3}	Canopy C_3 fraction leaf respiration (CO_2 flux)	μmol m^{-2} s^{-1}
R_{D4}	Canopy C_4 fraction leaf respiration (CO_2 flux)	μmol m^{-2} s^{-1}
R'_{D3}	Leaf respiration for a 100% C_3 canopy (CO_2 flux)	μmol m^{-2} s^{-1}
R'_{D4}	Leaf respiration for a 100% C_4 canopy (CO_2 flux)	μmol m^{-2} s^{-1}

TABLE A1. (*Continued*)

Symbol	Definition	Units
$R_{dQ_{10}}$	Q_{10} rate dark respiration	—
R_{hetero}	Soil heterotrophic respiration	μmol m^{-2} s^{-1}
R_n	Net radiation	W m^{-2}
R_{o1}	Quantity of water lost from site due to overland runoff	m
R_{roots}	Soil root respiration	μmol m^{-2} s^{-1}
r_{soil}	Soil surface resistance to evaporation	s m^{-1}
R_{soil}	Ground respiration	μmol m^{-2} s^{-1}
s_1	High temperature slope of inhibition of C_3 or C_4 V_{max0}	°C^{-1}
s_2	High temperature half inhibition of C_3 or C_4 V_{max0}	°C
s_3	Low temperature slope of inhibition of C_4 V_{max0}	°C^{-1}
s_4	Low temperature half inhibition of C_4 V_{max0}	°C
s_5	High temperature slope of inhibition of dark resp	°C^{-1}
s_6	High temperature half inhibition of dark resp	°C
$S\uparrow$	Site upward shortwave radiation	W m^{-2}
$S\downarrow$	Downward total shortwave radiation (S96: $F_{\text{a},\mu(0)}$)	W m^{-2}
$S\downarrow_{\text{PARfac}}$	PAR fraction of $S\downarrow$ adjustment factor	—
$S\uparrow_{\text{PAR}}$	Site upward PAR	W m^{-2}
$S\downarrow_{\text{PAR}}$	Site downward PAR	W m^{-2}
$S\uparrow_{\text{NIR}}$	Site upward NIR	W m^{-2}
$S\downarrow_{\text{NIR}}$	Site downward NIR	W m^{-2}
t	Time of day (from midnight local standard time)	hours
t_0	Time of solar noon (from midnight local standard time)	hours
$T_{\text{0–5cm}}$	Average soil temperature over 0–5-cm depth	°C
T_{10cm}	Soil temperature at 10-cm depth	°C
T_{50cm}	Soil temperature at 50-cm depth	°C
T_c	Canopy temperature	°C
T_d	Soil bottom (deep) temperature	°C
T_g	Soil surface (ground) temperature	°C
T_m	Above canopy (measurement height) dry-bulb temperature	°C
T_{skin}	Site skin temperature	°C
T_{wet}	Above canopy (measurement height) wet-bulb temperature	°C
u_m	Above canopy (measurement height) wind speed	m s^{-1}
V	Canopy cover fraction	—
V_{max0}	Rubisco rate capacity (at 25°C)	μmol m^{-1}
VWC	Volumetric water content	m^3 water m^3 soil
W_1	Fraction of saturated VWC of soil layer 1	—
W_2	Fraction of saturated VWC of soil layer 2	—
W_3	Fraction of saturated VWC of soil layer 3	—
W_{10cm}	VWC at 10-cm depth	—
W_{csp}	Linear water stress function, complete stress point	VWC
W_{isp}	Linear water stress function, initial stress point	VWC
w_{s1}	Low temp slope of inhibition of C_3 sink rate	°C^{-1}
w_{s2}	Low temp half inhibition of C_3 sink rate	°C
WUE	Water use efficiency	(mol CO_2) (mol H_2O)$^{-1}$
ϕ_s	Slope of soil subsurface drainage (mean topographic slope)	degrees
z_0	Roughness length	m
z_1	Canopy bottom height	m
z_2	Canopy top height	m
z_c	Canopy middle height	m
z_m	Canopy wind, temperature, flux measurement height	m
z_s	Ground roughness length	m
$\alpha_{\text{N,l}}$	Reflectance fraction, NIR, green (live) vegetation	—
$\alpha_{\text{N,d}}$	Reflectance fraction, NIR, nongreen (dead) vegetation	—
$\alpha_{\text{V,l}}$	Reflectance fraction, PAR, green (live) vegetation	—
$\alpha_{\text{V,d}}$	Reflectance fraction, PAR, nongreen (dead) vegetation	—
ϵ_3	C_3 intrinsic quantum efficiency	mol CO_2 mol^{-1} quanta
ϵ_4	C_4 intrinsic quantum efficiency	mol CO_2 mol^{-1} quanta
β_{ce}	Curvature coefficient C_3 sink or C_4 PEPcase colimitation	—
β_{pe}	Curvature coefficient light/rubisco colimitation	—
δ	Solar declination	deg
$\delta_{\text{N,l}}$	Transmittance fraction, NIR, green (live) vegetation	—
$\delta_{\text{N,d}}$	Transmittance fraction, NIR, nongreen (dead) vegetation	—
$\delta_{\text{V,l}}$	Transmittance fraction, PAR, green (live) vegetation	—
$\delta_{V,d}$	Transmittance fraction, PAR, nongreen (dead) vegetation	—
ΔM	Net change in total of surface intercepted water compartments	mm
ΔT	SiB2 simulation timestep	secs
ΔW_{soil}	Net change in total of water compartments	mm

TABLE A1. (*Continued*)

Symbol	Definition	Units
θ_s	Porosity (fraction of soil volume occupied at saturation), all soil layers	—
θ_{s1}	Porosity (fraction of soil volume occupied at saturation), soil layer 1	—
θ_{s2}	Porosity (fraction of soil volume occupied at saturation), soil layer 2	—
θ_{s3}	Porosity (fraction of soil volume occupied at saturation), soil layer 3	—
λ	Latitude	degrees
λE_c	Canopy total latent heat flux	W m^{-2}
λE_g	Ground total latent heat flux	W m^{-2}
λE_{ct}	Canopy bulk stomatal latent heat flux: transpiration	W m^{-2}
λE_{ct3}	Canopy C_3 fraction stomatal latent heat flux: transpiration	W m^{-2}
λE_{ct4}	Canopy C_4 fraction stomatal latent heat flux: transpiration	W m^{-2}
λE_m	Above canopy (measurement height) net site latent heat flux	W m^{-2}
λE_{ci}	Canopy latent heat flux: evaporation of intercepted water	W m^{-2}
λE_{gi}	Ground latent heat flux: evaporation of standing water	W m^{-2}
λE_{gs}	Ground latent heat flux: evaporation from soil layer 1	W m^{-2}
μ	Sine of the solar elevation angle	—
$\overline{\mu}$	Average μ for a day	—
Π	Leaf-level photosynthesis canopy integration factor	—
τ	Rubisco specificity ratio (carboxylase/oxygenase)	—
τ_{Q10}	Q_{10} Rubisco specificity ratio (carboxylase/oxygenase)	—
χ_L	Canopy leaf angle	—
Ψ_c	Soil water potential stress function, half inhibition point	m
Ψ_s	Water potential at saturation, all soil layers	m
Ψ_{s1}	Water potential at saturation, soil layer 1	m
Ψ_{s2}	Water potential at saturation, soil layer 2	m
Ψ_{s3}	Water potential at saturation, soil layer 3	m
ω_v	Scattering fraction of (unabsorbed) visible light (PAR) from the canopy	—

its unstressed value as soil water stress develops [S96, Eq. (C.17)]. A single value of f_w is used for the entire canopy. In SiB2v1.0, f_w is calculated based on soil layer 2 only (the ''rooting zone''). For the Tuned version, a separate value, $f_{w(i)}$, was calculated for each soil layer, using a linear approximation of the slope of a soil water stress curve (cf. Fig. 8):

$$f_{w(i)} = \frac{(W_{(i)}\theta_{s(i)}) - W_{\text{csp}}}{W_{\text{isp}} - W_{\text{csp}}}, \tag{A4}$$

where $f_{w(i)}$ is f_w for the ith soil layer ($0 < F_{w(i)} < 1$); W_{isp} is the water content of incipient water stress ($f_w = 1.0$); W_{csp} is the wilting point water content showing complete water stress ($f_w = 0.0$); $W_{(i)}$ is W for the ith soil layer; and $\theta_{s(i)}$ is θ_s for the ith soil layer (see Tables 1 and 2).

Then $f_{w(i)}$ is scaled by that layer's functional root capacity and combined with the other layers to produce an aggregate f_w for the canopy:

$$f_w = \sum_{i=1}^{3} f_{w(i)} f_{\text{root}(i)}, \tag{A5}$$

where $f_{\text{root}(i)}$ is f_{root} for the ith soil layer (see Table 1).

c. Hydrology

In SiB2v1.0 the maximum capacity of canopy interception and ground surface pools are set as constant values in the source code, and the depth of the top soil layer, D_1, is set to 2 cm. In the Calibrated and Tuned versions these were converted into variables allowing them to be assigned different values (see Table 1).

Table 2 lists the soil physics parameters. In SiB2v1.0 a single set of soil physics constants (θ_s, K_s, Ψ_s, and B) are used for all soil layers. In the Tuned version these constants were given separate values for each soil layer ($i = 1, 3$): $\theta_{s(i)}$, $K_{s(i)}$, $\Psi_{s(i)}$, and $B_{(i)}$. In the control and calibrated versions the maximum rate of infiltration of water into the soil was controlled by K_s. In the Tuned version infiltration was given a separate maximum conductivity constant, K_{infil}.

In SiB2v1.0 the roots are all in soil layer 2 (the rooting zone), and therefore all transpired water (E_{ct}) is extracted from layer 2. Tuned extraction of soil water was subdivided as a function of each soil layer's soil water stress ($f_{w(i)}$) and functional root fraction ($f_{\text{root}(i)}$). Each layer produced a single weighting factor, $f_{(i)}$. The $f_{(i)}$ from each soil layer were then normalized relative to the entire soil column and multiplied times E_{ct} to produce the contribution from each soil layer (i):

$$f_{(i)} = f_{w(i)} f_{\text{root}(i)}, \tag{A6a}$$

$$f_{E_{\text{ct}(i)}} = \frac{f_{(i)}}{\sum_{i=1}^{3} f_{(i)}}, \tag{A6b}$$

$$E_{\text{ct}(i)} = f_{E_{\text{ct}(i)}} E_{\text{ct}}, \tag{A6c}$$

where $f_{w(i)}$ is the soil moisture stress inhibition factor for the ith soil layer; $f_{\text{root}(i)}$ is the ith layer's functional root fraction (Table 1); $f_{E_{\text{ct}(i)}}$ is the normalized $f_{(i)}$; and $E_{\text{ct}(i)}$ is the portion of E_{ct} for the ith soil layer.

d. Soil respiration

SiB2v1.0 has a parameter for CO_2 flux from the soil, R_{soil} (root plus heterotroph respiration). This is not defined in S92. Randall et al. (1996) give an equation that can be calibrated to give R_{soil} such that the carbon budget for each grid box is seasonally balanced in GCM simulations of seasonal and meridional gradients of atmospheric CO_2. Lacking a full seasonal cycle, we could not use this approach here. We made use of an equation:

$$R_{soil} = a_{Rsoil}(0.135 + (0.054\ L_G)) \times (100 W_{10cm}) e^{[0.069(T_{10cm} - 25.0)]}, \quad \text{(A7)}$$

where R_{soil} is the estimated soil respiration (μmol m^{-2} s^{-1}); a_{Rsoil} is an arbitrary scaling constant introduced to allow the original sitewide equation to be scaled slightly to account for local site differences (Table 1); L_G is the green leaf area index; W_{10cm} is the volumetric soil moisture fraction at 10 cm estimated from (A9) with $x = 5$ and $z = 10$; and T_{10cm} is the soil temperature at 10 cm (°C) estimated from (A8) with $z = 10$. This equation is taken from Eq. (5) of Norman et al. (1992), who calibrated it to soil chamber measurements made at FIFE. The same equation was used in the Control, Tuned, and Calibrated simulations. Differences in soil respiration between the three versions resulted only from differences in predicted soil moisture and soil temperature.

e. Soil temperature at arbitrary depths

SiB2v1.0 only keeps track of soil temperature at the soil surface (T_g) and soil bottom (T_d). To approximate a temperature T_z (at any depth z cm) we used

$$T_z = T_d + (T_g - T_d) e^{-0.13z}. \quad \text{(A8)}$$

f. Soil water at arbitrary depths

SiB2v1.0 only keeps track of average water content in three layers. To produce a weighted average water content over any size range, x cm, centered at any depth, z cm, the SiB2 average water content values W_1, W_2, and W_3 (centered within their respective layer thicknesses D_1, D_2, and D_3) formed a water profile that we interpolated at run time. The average water content over the $(z - x/2, z + x/2)$ interval was taken as the trapezoidal integral divided by x:

$$W_z = \overline{W}(x, z, D_1, D_2, D_3, W_1, W_2, W_3). \quad \text{(A9)}$$

g. Soil evaporation

SiB2v1.0 has a standard r_{soil} equation with a W_1 dependence that is numerically identical to S96 [Eq. (35b)]. For our Calibrated and Tuned versions we used a functional form fitted to the FIFE site by S92b [Eq. (19)], where their r_{surf} equals our r_{soil}:

$$r_{soil} = e^{(a_{rsoil} - b_{rsoil} W_1)}, \quad \text{(A10)}$$

where a_{rsoil} is a regression constant (originally 8.206) and b_{rsoil} is a regression constant (originally 4.255) whose values from this work are listed in Table 1.

REFERENCES

Amthor, J. S., M. L. Goulden, J. W. Munger, and S. C. Wofsy, 1994: Testing a mechanistic model of forest-canopy mass and energy exchange using eddy correlation: Carbon dioxide and ozone uptake by a mixed oak–maple stand. *Aust. J. Plant Physiol.,* **21,** 623–651.

Avissar, R., and R. A. Pielke, 1989: A parameterization of heterogeneous land surfaces for atmospheric numerical models and its impact on regional meteorology. *Mon. Wea. Rev.,* **117,** 2113–2136.

Baldocchi, D., 1992: A Lagrangian random-walk model for simulating water vapor, CO_2 and sensible heat flux densities and scalar profiles over and within a soybean canopy. *Bound.-Layer Meteor.,* **61,** 113–144.

——, 1994: A comparative study of mass and energy exchange rates over a closed C_3 (wheat) and an open C_4 (corn) crop. II: CO_2 exchange and water use efficiency. *Agric. For. Meteor.,* **67,** 291–321.

Berry, J. A., and W. J. S. Downton, 1982: Environmental regulation of photosynthesis. *Photosynthesis*. Vol II: *Development, Carbon Metabolism and Plant Productivity,* Academic Press, 263–343.

Betts, A. K., and J. H. Ball, 1998: FIFE surface climate and site-average dataset 1987–89. *J. Atmos. Sci.,* **55,** 1091–1108.

——, ——, and A. C. M. Beljaars, 1993: Comparison between the land surface response of the European Centre model and the FIFE-1987 data. *Quart. J. Roy. Meteor. Soc.,* **119,** 975–1001.

Bjorkman, O., 1989: Some viewpoints on photosynthetic response and adaptation to environmental stress. *Photosynthesis,* W. R. Briggs, Ed., Alan R. Liss, 45–58.

Chaves, M. M., 1991: Effects of water deficits on carbon assimilation. *J. Exp. Bot.,* **42,** 1–16.

Chen, D. X., and M. B. Coughenour, 1994: GEMTM: A general model for energy and mass transfer of land surfaces and its application at the FIFE sites. *Agric. For. Meteor.,* **68,** 145–171.

Clapp, R. B., and G. M. Hornberger, 1978: Empirical equations for some soil hydraulic properties. *Water Resour. Res.,* **14,** 601–604.

Collatz, G. J., J. T. Ball, C. Grivet, and J. A. Berry, 1991: Physiological and environmental regulation of stomatal conductance, photosynthesis and transpiration: A model that includes a laminar boundary layer. *Agric. For. Meteor.,* **54,** 107–136.

——, M. Ribas-Carbo, and J. A. Berry, 1992: Coupled photosynthesis stomatal conductance model for leaves of C_4 plants. *Aust. J. Plant Physiol.,* **19,** 519–538.

Cooper, H. J., E. A. Smith, and W. L. Crosson, 1995: Limitations in estimating surface sensible heat fluxes from satellite radiometric skin temperatures. *J. Geophys. Res.,* **100,** 25 419–25 427.

Denning, A. S., I. Y. Fung, and D. A. Randall, 1995: Latitudinal gradient of atmospheric CO_2 due to seasonal exchange with land biota. *Nature,* **376,** 240–243.

——, G. J. Collatz, C. Zhang, D. A. Randall, J. A. Berry, P. J. Sellers, G. D. Colello, and D. A. Dazlich, 1996a. Simulations of terrestrial carbon metabolism and atmospheric CO_2 in a general circulation model. Part 1: Surface carbon fluxes. *Tellus,* **48B,** 521–542.

——, D. A. Randall, G. J. Collatz, and P. J. Sellers, 1996b: Simulations of terrestrial carbon metabolism and atmospheric CO_2 in a general circulation model. Part 2: Spatial and temporal variations of atmospheric CO_2. *Tellus,* **48B,** 543–567.

Famiglietti, J. S., E. F. Wood, M. Sivapalan and D. J. Thongs, 1992: A catchment scale water balance model for FIFE. *J. Geophys. Res.,* **97,** 18 997–19 007.

Field, C. B., and M. G. Goulden, 1988: Hydraulic lift: Broadening the sphere of plant-environment interactions. *Tree,* **3,** 189–190.

Gao, W., 1994: Atmosphere–biosphere exchange flux of carbon di-

oxide in a tallgrass pairie modeled with satellite spectral data. *J. Geophys. Res.,* **99,** 1317–1327.

Garratt, J. R., 1993: Sensitivity of climate simulations to land–surface and atmospheric boundary-layer treatments—A review. *J. Climate,* **6,** 419–449.

——, P. B. Krummel, and E. A. Kowalczyk, 1993: The surface energy balance at local and regional scales—A comparison of general circulation model results with observations. *J. Climate,* **6,** 1090–1109.

Gates, W. L., P. R. Rowntree, and Q. C. Zeng, 1990: Validation of climate models. *Climate Change: The IPCC Impacts Assessments,* W. J. McGegart, G. W. Sheldon, and D. C. Griffiths, Eds., Australian Govt. Publ. Service, 97–130.

Germann, P. F., and K. Beven, 1985: Kinematic wave approximation to infiltration into soils with sorbing macropores. *Water Resour. Res.,* **21,** 990–996.

Grant, R. F., and D. D. Baldocchi, 1992: Energy transfer over crop canopies: Simulation and experimental verification. *Agric. For. Meteor.,* **61,** 129–149.

——, P. Rochette, and R. L. Desjardins, 1993: Energy exchange and water use efficiency of field crops: Validation of a simulation model. *Agron. J.,* **85,** 916–928.

Hall, F. G., K. F. Huemmrich, S. J. Goetz, P. J. Sellers, and J. E. Nickeson, 1992: Satellite remote sensing of surface energy balance: Success, failures, and unresolved issues in FIFE. *J. Geophys. Res.,* **97,** 19 061–19 089.

Henderson-Sellers, A., A. J. Pitman, P. K. Love, P. Irannejad, and T. H. Chen, 1995: The project for intercomparison of land surface parameterization schemes (PILPS): Phases 2 and 3. *Bull. Amer. Meteor. Soc.,* **76,** 489–503.

Hope, A. S., 1992: Estimating the daily course of konza prairie latent heat fluxes using a modified terga model. *J. Geophys. Res.,* **97,** 19 023–19 031.

Johnson, I. R., J. J. Melkonian, J. H. M. Thornley, and S. J. Riha, 1991: A model of water flow through plants incorporating shoot/root ''message'' control of stomatal conductance. *Plant Cell Environ.,* **14,** 531–544.

Kaiser, W. M., 1987: Effects of water deficit on photosynthetic capacity. *Physiol. Plant.,* **71,** 142–149.

Kim, J., and S. B. Verma, 1990a: Components of surface energy balance in a temperate grassland ecosystem. *Bound.-Layer Meteor.,* **51,** 401–417.

——, and ——, 1990b: Carbon dioxide exchange in a temperate grassland ecosystem. *Bound.-Layer Meteor.,* **52,** 135–150.

——, and ——, 1991a: Modeling canopy photosynthesis: Scaling up from a leaf to canopy in a temperate grassland ecosystem. *Agric. For. Meteor.,* **57,** 187–208.

——, and ——, 1991b: Modeling canopy stomatal conductance in a temperate grassland ecosystem. *Agric. For. Meteor.,* **55,** 149–166.

——, C. Hays, S. Verma, and B. Blad, 1989: A preliminary report on LAI values obtained during FIFE by various methods. 27 pp. [Available from Center for Agricultural Meteorology and Climatology, UNL, P.O. Box 830728, Lincoln, NE 68583-0728.]

——, S. B. Verma, and R. J. Clement, 1992: Carbon dioxide budget in a temperate grassland ecosystem. *J. Geophys. Res.,* **97,** 6057–6063.

Knapp, A. K., 1985: Effect of fire and drought on the ecophysiology of andropogon geradii and panicum vergatum in a tallgrass prairie. *Ecology,* **66,** 1309–1320.

Liang, X., D. P. Lettenmaier, E. F. Wood, and S. J. Burges, 1994: A simple hydrologically based model of land surface water and energy fluxes for general circulation models. *J. Geophys. Res.,* **99,** 14 415–14 428.

MacPherson, J. I., R. L. Grossman, and R. D. Kelly, 1992: Intercomparison results for FIFE flux aircraft. *J. Geophys. Res.,* **97,** 18 499–18 514.

McMurtrie, R. E., R. Leuning, W. A. Thompson, and A. M. Wheeler, 1992: A model of canopy photosynthesis and water use incorporating a mechanistic formulation of leaf CO_2 exchange. *For. Ecol. Manag.,* **52,** 261–278.

Norman, J. M., R. Garcia, and S. B. Verma, 1992: Soil surface fluxes and the carbon budget of a grassland. *J. Geophys. Res.,* **97,** 18 845–18 854.

Pereira, J. S., and M. M. Chaves, 1993: Plant water deficits in mediterranean ecosystems. *Water Deficits Plant Responses from Cell to Community,* J. A. C. Smith and H. Griffiths, Eds., BIOS Scientific, 237–251.

Polley, H. W., J. M. Norman, T. J. Arkebauer, E. A. Walter-Shea, D. H. Greegor Jr., and B. Bramer, 1992: Leaf gas exchange of *Andropogon gerardii* vitman, *Panicum virgatum* 1., and *Sorghastrum nutans* (1.) Nash in a tallgrass pairie. *J. Geophys. Res.,* **97,** 18 837–18 844.

Quick, W. P., M. M. Chaves, R. Wendler, M. M. David, M. L. Rodrigues, J. A. Passaharinho, J. S. Pereira, M. D. Adcock, R. C. Leegood, and M. Stitt, 1992: The effect of water stress on photosynthetic carbon metabolism in four species grown under field conditions. *Plant Cell Environ.,* **15,** 25–35.

Randall, D. A., P. J. Sellers, J. A. Berry, D. A. Dazlich, C. Zhang, G. J. Collatz, A. S. Denning, S. O. Los, C. B. Field, I. Y. Fung, C. O. Justice, and C. J. Tucker, 1996: A revised land-surface parameterization (SiB2) for GCMs. Part III: The greening of the Colorado State University general circulation model. *J. Climate,* **9,** 738–763.

Saugier, B., and E. A. Ripley, 1975: A model of growth and water use for a natural grassland. *Proc. Summer Computer Simulation Conf.,* 945–953. [Available from Simulation Councils, 4838 Ronson Ct., Suite L, San Diego, CA 92111.]

Sellers, P. J., and F. G. Hall, 1992: FIFE in 1992: Results, scientific gains, and future research directions. *J. Geophys. Res.,* **97,** 19 091–19 109.

——, Y. Mintz, Y. C. Sud, and A. Dalcher, 1986: A simple biosphere model (SiB) for use within general circulation models. *J. Atmos. Sci.,* **43,** 305–331.

——, F. G. Hall, G. Asrar, D. E. Strebel, and R. E. Murphy, 1988: The First ISLSCP Field Experiment (FIFE). *Bull. Amer. Meteor. Soc.,* **69,** 22–27.

——, W. J. Shuttleworth, J. L. Dorman, A. Dalcher, and J. M. Roberts, 1989: Calibrating the simple biosphere model for Amazonian tropical forest using field and remote sensing data. Part I: Average calibration with field data. *J. Appl. Meteor.,* **28,** 727–759.

——, F. G. Hall, D. E. Strebel, R. D. Kelley, S. B. Verma, B. L. Markhame, B. L. Blad, D. S. Schimel, J. R. Wang, and E. Kanemasu, 1990: FIFE interim report February 1990. NASA/Goddard, 220 pp.

——, J. A. Berry, G. J. Collatz, C. B. Field, and F. G. Hall, 1992a: Canopy reflectance, photosynthesis and transpiration, III. *Remote Sens. Environ.,* **42,** 1–20.

——, M. D. Heiser, and F. G. Hall, 1992b: Relations between surface conductance and spectral vegetation indices at intermediate (100 m^{-2} to 15 km^{-2}) length scales. *J. Geophys. Res.,* **97,** 19 033–19 059.

——, F. G. Hall, G. Asrar, D. E. Strebel, and R. E. Murphy, 1992c: An overview of the First International Satellite Land Surface Climatology Project (ISLSCP) Field Experiment (FIFE). *J. Geophys. Res.,* **97,** 18 345–18 371.

——, M. D. Heiser, F. G. Hall, S. J. Goetz, D. E. Strebel, S. B. Verma, R. L. Desjardins, P. M. Schuepp, and J. I. MacPherson, 1995: Effects of spatial variability in topography, vegetation cover and soil moisture on area-averaged surface fluxes: A case study using the FIFE 1989 data. *J. Geophys. Res.,* **100,** 25 607–25 629.

——, D. A. Randall, G. J. Collatz, J. A. Berry, C. B. Field, D. A. Dazlich, C. Zhang, and G. D. Colello, 1996a: A revised land surface parameterization (SiB2) for atmospheric GCMs. Part I: Model formulation. *J. Climate,* **9,** 676–705.

——, S. O. Los, C. J. Tucker, C. O. Justice, D. A. Dazlich, G. J. Collatz, and D. A. Randall, 1996b: A revised land surface parameterization (SiB2) for atmospheric GCMs. Part II: The gen-

eration of global fields of terrestrial biophysical parameters from satellite data. *J. Climate,* **9,** 706–737.

——, L. Bounoua, G. J. Collatz, D. A. Randall, D. A. Dazlich, and S. Los, 1996c: Comparison of radiative and physiological effects of doubled atmospheric CO_2 on climate. *Science,* **271,** 1402–1406.

Sharkey, T. D., and M. R. Badger, 1982: Effects of water stress on photosynthetic electron transport, photophosphorylation, and metabolite levels of *Xanthium strumarium* mesophyll cells. *Planta,* **156,** 199–206.

Stewart, J. B., and S. B. Verma, 1992: Comparison of surface fluxes and conductances at two contrasting sites within the FIFE area. *J. Geophys. Res.,* **97,** 18 623–18 628.

Strebel, D. E., D. R. Landis, K. F. Huemmrich, and B. W. Meeson, 1994: *Collected Data of the First ISLSCP Field Experiment, Volume 1: Surface Observations and Non-Image Data Sets*. NASA, CD-ROM. [Available from PLDS, Code 923, NASA/GSFC, Greenbelt, MD 20771.]

Tardieu, F., and W. J. Davies, 1993a: Integration of hydraulic and chemical signalling in the control of stomatal conductance and water status of droughted plants. *Plant Cell Environ.,* **16,** 341–349.

——, and ——, 1993b: Root-shoot communication and whole-plant regulation of water flux. *Water Deficits Plant Responses from cell to Community,* J. A. C. Smith and H. Griffiths, Eds., BIOS Scientific, 237–251.

Tardieu, F., N. Katerji, O. Bethenod, J. Zhang, and W. J. Davies, 1991: Maize stomatal conductance in the field: Its relationship with soil and plant water potentials, mechanical constraints and ABA concentration in the xylem sap. *Plant Cell Environ.,* **14,** 121–126.

——, J. Zhang, and D. J. G. Gowing, 1993: Stomatal control by both [ABA] in the xylem sap and leaf water status: A test of a model for droughted or ABA-fed field-grown maize. *Plant Cell Environ.,* **16,** 413–420.

Verma, S. B., J. Kim, and R. J. Clement, 1989: Carbon dioxide, water vapor and sensible heat fluxes over a tallgrass prairie. *Bound.-Layer Meteor.,* **46,** 53–67.

——, ——, and ——, 1992: Momentum, water vapor, and carbon dioxide exchange at a centrally located prairie site during FIFE. *J. Geophys. Res.,* **97,** 18 629–18 639.

——, P. J. Sellers, C. L. Walthall, F. G. Hall, J. Kim, and S. J. Goetz, 1993: Photosynthesis and stomatal conductance related to reflectance on the canopy scale. *Remote Sens. Environ.,* **44,** 103–116.

Vining, R. C., and B. L. Blad, 1992: Estimation of sensible heat flux from remotely sensed canopy temperatures. *J. Geophys. Res.,* **97,** 18 951–18 954.

Viterbo, P., and C. M. Beljaars, 1995: An improved land surface parameterization scheme in the ECMWF model and its validation. *J. Climate,* **8,** 2716–2748.

Walter-Shea, E. A., B. L. Blad, C. J. Hays, M. A. Mesarch, D. W. Deering, and E. M. Middleton 1992: Biophysical properties affecting vegetative canopy reflectance and absorbed photosynthetically active radiation at the FIFE site. *J. Geophys. Res.,* **97,** 18 925–18 934.

Wofsy, S. C., M. L. Goulden, J. W. Munger, S.-M. Fan, P. S. Bakwin, B. C. Daube, S. L. Bassow and F. A. Bazzaz, 1993: Net exchange of carbon dioxide in a mid-latitude forest. *Science,* **260,** 1314–1317.

Wood, E. F., and V. Lakshmi, 1993: Scaling water and energy fluxes in climate systems: Three land–atmosphere modeling experiments. *J. Climate,* **6,** 839–857.